A Bayes Risk-Based Cost Function to Allocate Scan Time for Object Detection

Master Thesis

E. van Veldhuijzen

A Bayes Risk-Based Cost Function to Allocate Scan Time for Object Detection

by

E. van Veldhuijzen

to obtain the degree of Master of Science
in Electrical Engineering
at the Delft University of Technology,
to be defended publicly on Friday October 6, 2023 at 13:30 AM.

Student number:	4480198	
Project duration:	May 1, 2022 – October 6, 2023	
Thesis committee:	Prof. dr. O. Yarovyi,	TU Delft, responsible professor
	dr. ir. J.N. Driessen,	TU Delft, supervisor
	dr. N.J. Myers,	TU Delft

An electronic version of this thesis is available at http://repository.tudelft.nl/.

TU Delft

Abstract

Advancements in radar technology such as phased array antennas, digital beamforming, and adaptable waveform generation have led to the flexibility in controlling radar resources such as scan time, beamwidth and bandwidth during a radar mission. This new flexibility has led to a new research topic, radar resource management.

Radar resource management involves the allocation of radar resources in order to achieve the highest performance in a radar mission. This thesis focuses on a specific scenario where a radar is tasked with deciding multiple object presence decisions located at multiple scan directions. The resource considered is the scan time allocated to each scan direction.

To optimally allocate the scan time over the scan directions, a cost function is formulated, where the expected performance of an individual decision of an object being present or absent is formulated as the expected Bayes risk. The expected performance of all individual decisions in the same scan direction, are summed to obtain an expected task performance. The global performance at the system level is formulated using two approaches. The *Sum* approach formulates a cost function at the system level as the sum of the expected cost of each task. The *Max* approach formulates a cost function that minimizes the maximum of all expected task costs.

Simulations have been performed to demonstrate the flexibility of the *Sum* and *Max* approach to adapt the scan time allocation based on different scenarios, including multiple object presence decisions per scan direction, sequential measurements, and a birth-death process regarding the presence of an object over time. Simulations demonstrate that using the *Sum* and *Max* approaches for the allocation of scan time results in an improved performance compared to the uniform distribution of the scan time resource over all scan directions.

Acknowledgements

I would like to thank my supervisor dr. ir. Hans Driessen for guiding me through this thesis, his patience, and support. Furthermore, I would like to thank Prof. dr. Olexander Yarovyi and dr. Nitin Myers for being the exam committee members for my thesis defence.

Furthermore, I would like to thank my girlfriend Stefanie, my parents Johan and Margreeth, my brothers Stefan and Richard, my sisters-in-law Denise and Tirza, for their emotional support during my time in Delft, especially during the final stage of my masters. A special thanks goes to my little nephews Zev, Noud and Dex for being able to always put a smile on my face.

List of Figures

List of Tables

Contents

1 Introduction

A radar is a system that is able to observe its surrounding environment by emitting electromagnetic waves (signal) and analysing the reflections on objects. The relative insensitivity of performance degradation compared to other sensor technologies such as a camera or lidar due to weather conditions such as rain, smoke, dark (absent of sunlight) makes radar a popular choice in a wide range of surveillance applications.

In airborne ground surveillance, radar is used to search for and track objects on the ground from a plane. In weather surveillance, radar is used to predict weather conditions such as the intensity of rainfall or snowfall. In air traffic control, radar is used to monitor the movement of airplanes. In security systems, radar is used to detect humans and vehicles that are trespassing. The examples given are only a small subset of the total number of applications where a surveillance radar is used.

Traditionally, radars used mechanically rotating parabolic antennas. The parabolic antenna results in a strong focused signal in the direction of the axis of symmetry of the parabolic shape. The disadvantage of radars using such antennas is that the direction of signal focus depends on the mechanical orientation of the parabolic antenna. Changing the direction of signal focus requires mechanically rotating the antenna.

Recently, phased array radar has gained popularity, where a phased array antenna is used to steer the signal focus electronically. A phased array antenna has a maximum angle coverage of 180°, but is lower in practice. To obtain an angle coverage of 360°, multiple phased array antennas or a single phased array antenna that is capable of mechanical rotation are required. The advantage of electronically steering the scanning angle is the ability to change the direction of signal focus almost instantaneously. In mechanically rotating parabolic antennas, the scan direction pattern is limited to clockwise or counterclockwise. The flexibility of steering the angle for phased array radars angle can be exploited in surveillance applications. Consider an air traffic controller setting where two airplanes are tracked. If the two airplanes are present in different scan directions with respect to the radar, but within the angle coverage of the phased array radar, a mechanically rotating parabolic antenna is forced to rotate clockwise or counterclockwise when the radar switches between which object to track. This results in an effective scan time on the two airplanes considerably lower than 100%. In such an application, a phased array radar would allow for an almost instantaneous change in the scan angle, resulting in an effective scan time allocation close to 100%.

Furthermore, the implementation of digital beamforming allows a radar to control multiple beams simultaneously for different directions with an adjustable beamwidth. Consider the scenario in which an airport wants to have an overview of drones near an airport. The first task is to be aware of the presence of drones. The second task is to accurately follow the drones to locate and predict their movement. If for both tasks a relatively wide beam is used, the drones will be detected relatively fast. However, the location and trajectory prediction will be less accurate. When a relatively narrow beam is used, the location and trajectory prediction will increase in performance, but it could take too long before the drones are found. This example illustrates that different radar tasks benefit from different radar beamwidth. The development in radar technology by using digital beamforming introduces flexibility in radar parameters such as beamwidth. Using digital beamforming, a radar can use a wide beamwidth to scan the whole search area relative fast, and use a narrow beamwidth to locate and predict the trajectory of the drones found.

Where in the past only a single type of waveform was used in a radar, nowadays radars have the ability to quickly switch to a different type of waveform during operation. The ability to change waveforms allows the radar to quickly adapt to a changing radar environment. Consider a radar surveillance scenario where the coastal guard is interested in trespassing boats. The transmitted waveforms will reflect strongly on the sea, resulting in a low signal-to-clutter ratio, where the power resulting from

signal reflections on the sea is referred to as clutter power. Being able to adapt the transmitted waveforms based on the current behavior of the sea will lead to better radar performance in such scenarios. [1]

The newly introduced degrees of freedom for the radar resources as mentioned above are a subset of the total development within radar technology, but demonstrate the potential of increased radar mission performance. The actual improved radar mission performance depends on the ability of the radar to choose the resources such that it maximizes the performance.

1.1 Research goal and objectives

This research focuses on a scenario in which the radar is tasked with multiple decisions regarding the presence of an object. The performance of each decision benefits from more allocated resources. The resource considered is the scan time, which is divided over all scan directions that contain cells that require an object presence decision. Given that each object presence decision has improved performance as more scan time is allocated to that object, a trade-off is required to balance the performance of the object presence decisions.

The main goal of this research was to formulate a cost function that predicts the expected detector performance of multiple object presence decisions as a single function of the scan time allocated to each scan direction, which includes flexibility for the radar user to prioritize individual detector decisions.

To achieve this goal, the following objectives have been formulated:

- Review of literature on the formulation of cost functions to allocate resources for object detection
- Formulating cost performances for individual object presence decisions that have a direct interpretation at the application level
- Formulate potential cost functions at the system level that take into account the cost of individual object presence decisions
- Simulating radar measurements, allocating the scan time over the scan directions by minimizing the found cost functions at the system level, to explain and compare performances

1.2 Outline of the thesis

This thesis consists of 7 chapters. Chapter 1 introduces the research topic and formulates the research goal and objectives. Chapter 2 reviews the relevant literature on the research topic and identifies a research gap. Chapter 3 derives explicit equations for the performance of individual object presence decisions using common detectors, assuming simplified measurement models. Chapter 4 uses the performance equations of Chapter 3 to formulate costs for individual object decisions and extends this to a cost function at the system level for a scenario with a single object presence decision per scan direction. Chapter 5 generalizes the scenario in Chapter 4 and reformulates the cost of individual decisions and the cost function at the system level. Chapter 6 simulates the allocation of scan time and corresponding detector choices, using the scenarios and cost functions formulated in Chapters 4 and 5 and explains the choices made and compares performance. Chapter 7 concludes the research and gives recommendations for the potential continuation of this work.

2 Literature Review

This chapter presents a review of the literature on the formulation of an objective function at the system level to allocate sensor resources to improve the performance of detecting potential objects. The lack of sufficient literature on this topic led to the decision to expand the search to include literature that had a different main topic, but included the formulation of a utility or cost function to allocate resources to detect objects.

The literature is divided into two different approaches to formulate an objective function at the system level. Both approaches share that a performance, which is a function of the available resource, is formulated for each individual spatial coordinate within the considered search volume or area. The formulation of the performance of individual spatial coordinates for the literature reviewed in this chapter involves the quantity of expected undetected objects or the expected detector performance associated with object detection.

Section 2.1 presents the literature that formulates a cost or utility function at the system level by the sum of local costs or utilities. Section 2.2 presents the literature that formulates a cost or utility function at the system level by the maximum or minimum of subsets of local costs or utilities.

2.1 Objective functions at the system level based on the summation of task objectives

The literature reviewed in this section obtains the performance at the system level by the sum or integral of local performances. When the local performance is formulated as a cost, the distribution of resources is found by minimizing the sum of the local performances. When local performance is formulated as a utility, the distribution of resources is found by maximizing the sum of local utilities.

Williams [2] considered a scenario with a discretized search volume. Each cell within the search volume had an intensity of undetected objects, representing the expected number of undetected objects in that cell. The intensity of undetected objects was modeled by a Poisson process that included the birth, death, and movement of objects. The posterior undetected object intensity was modeled by multiplying the prior undetected object intensity by the probability of a missed detection, while the probability of a false alarm was fixed. In order to distribute the scan time budget over different scan directions, a cost function was formulated at the system level by minimizing the sum of the cost of individual cells. The cost of an individual cell was formulated as a cost coefficient C multiplied by the posterior undetected object intensity. Resulting in a cost function at the system level that distributes the scan time budget to minimize the total expected cost due to undetected objects. This cost function was evaluated for both the prediction of a single scan and multiple scans ahead. Increasing the prediction horizon of the cost function resulted in a lower expected cost. The lower cost was obtained by allocating the budget more sparse over the scan directions.

Boström-Rost et al. [3] considered a scenario where the radar was tasked to search for undetected objects and simultaneously track detected objects. The radar observation area was modeled as continuous, with each point in space assigned a multiobject density using the Poisson multi-Bernoulli mixture filter. The detection component of the multiobject density represented the undetected object intensity. The cost function at the system level consisted of the sum of the utility of track cost and a weighted detection performance. The weighting allowed the radar user to trade off the importance at the system level of the track and detection performance. The detection performance at a single point in the observation volume was the posterior undetected object intensity, assuming a Neyman-Pearson detector. The detection performance at the system level was modeled as the surface integral of the posterior undetected object intensity over the entire observation area. The detection component of the cost function at the system level minimized the posterior number of undetected objects.

Collins et al. [4] considered a wide area surveillance scenario, where the radar was tasked to track detected objects and search for undetected objects, including classification. The observation area was discretized into cells. The cost function at the system level is the sum of the track and search cost. The available resource was the scan time, where multiple scans were predicted ahead. The cost function at the system level consisted of the sum of the cost of the track and the combined detection and classification performance. The detection and classification performance in individual cells was formulated as a cost multiplied by the expected number of undetected objects multiplied by an entropy term related to the probabilities of an object belonging to each class type. The detection and classification cost at the system level was obtained by the sum of the cost of individual cells.

Hoffmann and Charlish [5] considered an airborne scenario. The search volume is discretized into cells. Both the velocity and height of an object were included in this research. The scan time budget is allocated over multiple scan directions, based on a utility function. Each scan direction is formulated as a utility task. The utility of a task is formulated as the maximum range that has a probability of detection greater than 0.9 using a Neyman-Pearson detector. The utility function at the system level is obtained by the sum of each individual task.

2.2 Objective functions at the system level based on the maximum of task objectives

The literature reviewed in this section has a similar approach. Given the local performances of individual spatial coordinates, all local performances sharing the same scan direction are summed to obtain a task performance. Performance at the system level is evaluated by the maximum utility of individual tasks.

White et al. [6] considered a scenario in which the radar was tasked with object detection and tracking. The search area was discretized into cells. A fixed budget ratio was allocated to the detection and tracking task, with the ratio specified by the radar user. Each cell consisted of an undetected object intensity. The available budget was both the scan direction and the beamwidth. The entire budget was allocated to object detection or tracking, with tracking using a narrower bandwidth. The detection task chose the scan direction that resulted in the highest expected number of new detected objects.

Matthiessen [7] focused on the efficient beam scanning, energy and time allocation. The radar was tasked with searching for undetected objects. The search area was discretized into cells. The available budget was the power, scan direction, and the number of scans used. The entire budget is allocated to the direction that maximizes the number of newly detected objects. The allocated power was determined by maximizing $\frac{\Delta\text{newly detected objects}}{\Delta S/N}$ with S/N the signal-to-noise ratio.

Flint et al. [8] considered a path planning algorithm for autonomous UAV's searching for objects while navigating through an environment containing threats. The search area is discretized into cells. The UAV scans the current position cell. The available search budget is the future UAV position. The future position is the cell that is expected to produce the highest number of newly detected objects, using a Neyman-Pearson detector.

Wang et al. [9] designed a sensor management scheme to detect potential objects, emphasizing the number of scans for optimal budget allocation. The search area was discretized into cells. The detector chosen is the minimum probability of error. This paper introduces an additional cost to take an extra measurement before making a detector decision. The number of optimal scans is a trade-off between the reduced probability of an error after multiple scans, at the cost of the additional cost per scan of delaying a detector decision. Each cell has its own cost, inflicted by an incorrect detector decision, assigned by the radar user. At the system level, the cost function determines the next scan direction by choosing the cell with the lowest expected cost.

2.3 Research gap

The considered papers allocate the resource by minimizing the expected cost or maximizing the expected utility functions. To unify both approaches, this section considers the equivalence of maximizing the utility and minimizing the negative utility. With the negative utility interpreted as a cost, each paper now allocates the budget by minimizing a cost function.

All articles are categorized on the basis of two criteria:

- The ability of the radar user to provide costs to quantify preferences of individual object presence decisions
- The mapping approach of individual cell performances to a single cost function at the system level

Using the earlier definition of the sum of all the cell performances in a single scan direction as the task performance, the second criteria is categorized in the following two approaches:

- A performance at the system level using the sum of task performances, referred to as the *Sum* approach
- A performance at the system level using the maximum of all task performances, referred to as the *Max* approach

The categorization is shown in table 2.1, which categorizes the literature based on the ability of the radar user to quantify costs within the cost function at individual decisions and whether the *Sum* or *Max* approach is used at the system level. Table 2.1 shows:

Category	Cost	No cost
Sum	[2] [4]	[3] [5]
Max	[9]	[6] [7] [8]

Table 2.1: Categorization of literature

- The literature's lack of a preference between the *Sum* and *Max* approach
- A relative shortage of literature that provides a cost function at the system level which enables the user to provide costs at individual cells.

This thesis aims to fill this research gap by formulating cost functions at the system level both using the *Sum* and *Max* approach, while enabling the user to provide costs at individual cells, to prioritize the performance of individual object decisions.

3 Radar-based object detection

This chapter first gives a short radar introduction in Section 3.1. The detector makes the hypothesis decisions in a radar, which is considered in Section 3.2. Subsections 3.2.1 and 3.2.2 formulate the measurement equations for the assumed models under both object presence and absence. Subsection 3.2.3 derives the detector performance equations without assuming a specific type of detector. Subsections 3.2.4, 3.2.5, 3.2.6 and 3.2.7 derive explicit detector performance equations for the Neyman-Pearson, minimum probability of error, minimax and minimum Bayes risk detector, respectively. This chapter emphasizes the influence of the scan time on the object presence decision performance.

3.1 Radar

A radar is a system that observes the spatial environment of interest surrounding the radar, defined as the search volume of the radar. The radar antenna emits propagating electromagnetic (EM) waves into the radar search volume. The interaction of EM waves with objects of interest causes a fraction of the EM wave energy to reflect back to the radar, termed the reflected signal. The reflected signal received at the radar is analyzed to extract information of the object such as range, (Doppler) velocity, object class, and the presence of that object.

Complicated electronic circuits are involved in the radar receiver to analyze the received signals. Electronic circuits generate noise as a result of internal thermal noise. Thermal noise is generated independently of the presence of a received signal.

Object that aren't of interest to the radar also reflect energy back to the radar and are referred to as clutter. Clutter can have similar reflection characteristics compared to objects, making it difficult for radars to distinguish between clutter and objects. This thesis assumes the absence of clutter and other forms of interference, such as jamming and environmental electromagnetic radiation noise.

The detector within the radar is tasked with deciding whether the received signal consists of only thermal noise or thermal noise combined with a reflected signal. The ability of the detector to distinguish between the case of thermal noise or thermal noise combined with a reflected signal from objects of interest depends on many radar parameters and physical phenomena. This thesis focuses on the effect of:

- The effect of the allocated scantime to a specific scan direction within a single scan
- The range of a potential object

The effect of the allocated scan time to a specific scan direction affects both the thermal noise and the reflected signal. The thermal noise is uncorrelated, resulting in a thermal noise power with a linear dependence on the allocated scantime. The signal reflected from an object is assumed to be correlated throughout the scan, resulting in a signal power with a quadratic dependency on the allocated scan time.

The range of a potential object affects only the signal power, the noise power is unaffected. The relation between the signal power received and the range of a potential object is given by the radar range equation.

The Radar Range Equation has many forms, which relate the received signal to interference power ratio taking into account physical dependencies such as antenna gain, receiver thermal noise, wavelength and range of the object. A full chapter on the Radar Range equation can be found in Chapter 2 of [10]. This chapter focuses on the relevant dependencies considered in this thesis:

$$SNR \propto \frac{\sigma}{R^4} \tag{3.1}$$

Where σ is the radar cross-section $[m^2]$ (RCS). R $[m]$ is the radial distance (range) between the radar and the object.

A higher SNR results in better detector performance. The relationship between SNR and the range in equation 3.1 results in a better detector performance for objects at shorter range compared to objects at larger range.

Section 3.2 explains how a detector decides on the presence or absence of an object.

3.2 Detector

The detector decides whether an object is present or absent by hypothesis testing. The presence or absence requires two hypothesis to be tested and compared:

H_1 : Object is present
H_0 : Object is absent

The received signal has different statistical properties under H_0 and H_1. This enables the detector to base the object presence decision on the statistical properties of the received signal. The difference in statistical properties enables the radar to gather evidence for either hypothesis by performing a measurement on the potential object.

When an object is absent, the statistical properties of thermal white noise fully characterize the received signal. When an object is present, the combined statistical properties of the thermal white noise and object reflection characterize the received signal.

Measurements can be real-valued or complex-valued. It is assumed that a square law detector is used so that the measurements are continuous and real valued, noted by $z \in \mathbb{R}$. Under hypotheses H_0 and H_1, the probability density functions that describe the measurements are $p(z/H_0, T)$ and $p(z/H_1, R, T)$, described in Subsections 3.2.1 and 3.2.2, to relate the measurement z to either hypothesis.

3.2.1 Object absent measurement model

When an object is absent, measurements are assumed to be generated by interference only. It is assumed that the interference is dominated by internal thermal noise. The probability density function of the internal thermal noise voltage is modeled by a zero mean Gaussian distribution

A detector that analyzes the voltage of a received signal is called a linear detector, while a detector that analyzes the power of a received signal is called a square law detector. [10] states in Subsection 15.4.1 that, for a square-law detector, the power output of a coherent radar receiver for thermal noise is modeled by an exponential distribution. The power of the signal in the receiver is defined as $z \in \mathbb{R}_{\geq 0}$. Under hypothesis H_0, the probability density function that describes the measurement is the following:

$$p(z, H_0, T) = \frac{1}{T\sigma_n^2} e^{-\frac{z}{T\sigma_n^2}} \tag{3.2}$$

and the cumulative distribution function for a threshold γ is:

$$p(z \leq \gamma / H_0, T) = 1 - e^{-\frac{\gamma}{T\sigma_n^2}} \tag{3.3}$$

with σ_n^2 the noise variance normalized with respect to scan time. The product $T\sigma_n^2$ is the noise variance for an allocated scan time T on the object. The uncorrelated nature of thermal noise results in a linear dependence on the scan time for the noise variance.

3.2.2 Object present measurement model

For the case where an object is present, the measurements are generated by the superposition of noise as characterized in Section 3.2.2 and reflections of the object. For simplicity, it is assumed that an object consist of a large number of scatterers with approximately equal RCS and uniformly distributed phases on $(0, 2\pi)$. [10] states that the RCS of the object is characterized by an exponential distribution. During the scan interval T, the object model assumes coherent processing. The noise variance of the normalized reflected signal with respect to scan time T and range R is defined as σ_s^2, resulting in a variance of the reflected signal of $\frac{T^2\sigma_s^2}{R^4}$.

It is assumed that the noise and the reflected signal power are independent, resulting in a superposition of the variances for the probability density function.

Under the hypothesis H_1, the probability density function that describes the measurement is:

$$p(z/H_1, R, T) = \frac{1}{T\sigma_n^2 + T^2\frac{\sigma_s^2}{R^4}} e^{-\frac{z}{T\sigma_n^2 + T^2\frac{\sigma_s^2}{R^4}}} \tag{3.4}$$

and the cumulative distribution function for a threshold γ is described as:

$$p(z \leq \gamma/H_1, R, T) = 1 - e^{-\frac{\gamma}{T\sigma_n^2 + T^2\frac{\sigma_s^2}{R^4}}} \tag{3.5}$$

The assumed coherent processing for the object component of the measurement model is reflected in the quadratic dependence on T for the variance of the signal.

The detector's ability to correctly decide on the existence of the object depends on $SNR(R, T)$. $SNR(R, T)$ is defined as $\frac{\text{Signal power}}{\text{Noise power}} = T\frac{\frac{\sigma_s^2}{R^4}}{\sigma_n^2}$. The amount of scan time available for a measurement has a direct influence on $SNR(R, T)$.

In the limit of $\lim_{T\to\infty}$, the probability density function assuming H_1 is:

$$\lim_{T\to\infty} p(z/H_1, R, T) \approx \lim_{T\to\infty} \frac{1}{T^2\frac{\sigma_s^2}{R^4}} e^{-\frac{z}{T^2\frac{\sigma_s^2}{R^4}}} \tag{3.6}$$

Equation 3.6 does not depend on the noise power as the signal power dominates. Therefore, increasing the available budget for a measurement causes the measurement models under H_0 and H_1 to diverge, as the received object power dominates over the noise power, resulting in a detector with statistically better performance.

In the limit of $\lim_{T\to 0}$, the probability density function assuming H_1 is:

$$\begin{aligned} \lim_{T\to 0} p(z/H_1, R, T) &\approx \lim_{T\to 0} \frac{1}{T\sigma_n^2} e^{-\frac{z}{T\sigma_n^2}} \\ &= \lim_{T\to 0} p(z/H_0, T) \end{aligned} \tag{3.7}$$

Equation 3.7 does not depend on the signal power in the limit $\lim_{T\to 0}$, the noise power dominates over the signal power.

For small T, the object absent and object present models will converge, as the signal variance decreases quadratic with decreasing scan time, while the noise variance decreases linearly with decreasing scan time.

Equations 3.4 and 3.5 rarely describe practical radar scenarios, as mentioned in [10]. However, the measurement models in this thesis are used as tools to obtain the detector equations in Subsection 3.2.3, justifying the use of equations 3.2 and 3.4 in order to simplify the detector equations in Subsection 3.2.3.

3.2.3 Detector decisions

The detector is the mechanism within a radar that decides which hypothesis is accepted, which is a correct or incorrect decision. For a binary hypothesis testing problem, four different decision events can occur.

When an object is present and the radar declares H_0, the event is defined as a miss, with the corresponding probability $P_{miss}(R,T)$. When the object is present and the radar accepts H_1, the event is defined as a detection, with corresponding probability $P_{det}(R,T)$. When an object is absent and the radar accepts H_0, the event is defined as a correct rejection (of the Null hypothesis), with the corresponding probability $P_{rej}(R,T)$. When the object is absent and the radar accepts H_1, the event is defined as a false alarm, with corresponding probability $P_{fa}(R,T)$. The detectors considered in this chapter are based on the probabilities of the four events described above.

The decision whether to accept H_0 or H_1 is based on whether the measurement exceeds a threshold γ. The threshold γ is based on desired characteristics of the events $P_{fa}(R,T)$, $P_{rej}(R,T)$, $P_{det}(R,T)$ and $P_{miss}(R,T)$. Given a threshold γ, [11] states that the optimal decision is made by evaluating whether the likelihood ratio $\frac{p\left(z/H_1,R,T\right)}{p\left(z/H_0,T\right)}$ exceeds γ:

$$\begin{aligned}\frac{p\left(z/H_1,R,T\right)}{p\left(z/H_0,T\right)} &= \frac{\sigma_n^2}{\sigma_n^2+T\frac{\sigma_s^2}{R^4}}e^{\frac{z}{T\sigma_n^2}-\frac{z}{T\sigma_n^2+T^2\frac{\sigma_s^2}{R^4}}} \\ &\underset{H_0}{\overset{H_1}{\gtrless}} \gamma\end{aligned} \tag{3.8}$$

Equation 3.8 states that when the measurement z is at least a factor $\frac{1}{\gamma}$ more likely to be generated by the model corresponding to H_1 than by the model corresponding to H_0, the detector will accept H_1. The value of γ has a direct influence on the probabilities of $P_{fa}(R,T) = P\Big(L(z) > \gamma/H_0,R,T\Big)$, $P_{rej}(R,T) = P\Big(L(z) < \gamma/H_0,R,T\Big)$, $P_{det}(R,T) = P\Big(L(z) > \gamma/H_1,R,T\Big)$, and $P_{miss}(R,T) = P\Big(L(z) < \gamma/H_1,R,T\Big)$.

For example, when $\gamma >> 1$, the detector will produce a relatively low $P_{fa}(R,T)$ and high $P_{rej}(R,T)$, but this is traded off by a relative high $P_{miss}(R,T)$ and low $P_{det}(R,T)$. On the contrary, choosing $\gamma << 1$ will result in relatively low $P_{miss}(R,T)$ and high $P_{det}(R,T)$ with relative high $P_{fa}(R,T)$ and low $P_{rej}(R,T)$.

Therefore, the threshold parameter γ allows the detector to increase the probability of making a correct decision for a given hypothesis by decreasing the probability of making a correct decision given the other hypothesis.

Equation 3.8 is rewritten in equation 3.9 so that measurement z is the only term on the left side of the equation. This enables the detector to directly compare the measurement to a modified threshold $\gamma'(R,T)$.

$$\begin{aligned}z &\underset{H_0}{\overset{H_1}{\gtrless}} log\left(\gamma\left(1+SNR(R,T)\right)\right)\frac{T\sigma_n^2+T^2\frac{\sigma_s^2}{R^4}}{SNR(R,T)} \\ &= \gamma'(R,T)\end{aligned} \tag{3.9}$$

The dependency of $\gamma'(R,T)$ on T is a result of the dependency on T for the measurement models $p\left(z/H_0,T\right)$ and $p\left(z/R,H_1,T\right)$. As T increases, $p\left(z/R,H_1,T\right)$ is likely to create a relatively larger z compared to $p\left(z/H_0,T\right)$, causing $\gamma'(R,T)$ to increase.

γ is still undetermined in equation 3.9. Sections 3.2.4, 3.2.5 and 3.2.7 determine γ for different common detector frameworks, using the definitions of $P_{fa}(R,T)$, $P_{rej}(R,T)$, $P_{det}(R,T)$ and $P_{miss}(R,T)$ as written below.

The probability of a false alarm as function of R and T is: [11]

$$\begin{aligned} P_{fa}(R,T) &= P\Big(L(z) > \gamma / H_0, R, T\Big) \\ &= \int_{\{z:L(z)>\gamma\}} p(z/H_0,T)dz \\ &= e^{-\frac{\gamma'(R,T)}{T\sigma_n^2}} \\ &= e^{-log\Big(\gamma\big(1+SNR(R,T)\big)\Big)\frac{SNR(R,T)+1}{SNR(R,T)}} \end{aligned} \tag{3.10}$$

The probability of a correct rejection as function of R and T is:

$$P_{rej}(R,T) = 1 - P_{fa}(R,T) \tag{3.11}$$

The probability of a missed detection as function of R and T is: [11]

$$\begin{aligned} P_{miss}(R,T) &= P\Big(L(z) < \gamma / H_1, R, T\Big) \\ &= \int_{\{z:L(z)<\gamma\}} p(z/H_1,R,T)dz \\ &= 1 - e^{-\frac{\gamma'(R,T)}{T\sigma_n^2 + T^2\frac{\sigma_s^2}{R^4}}} \\ &= 1 - e^{-log\Big(\gamma\big(1+SNR(R,T)\big)\Big)\frac{1}{SNR(R,T)}} \end{aligned} \tag{3.12}$$

The probability of a detection as function of R and T is:

$$P_{det}(R,T) = 1 - P_{miss}(R,T) \tag{3.13}$$

3.2.4 Neyman-Pearson

A Neyman-Pearson detector maximizes $P_{det}(R,T)$ by fixing $P_{fa}(T)$ to a desired value α. The threshold is determined by [11]:

$$\begin{aligned} P_{fa}^{NP}(T) &= 1 - e^{-\frac{\gamma^{NP}(T)}{T\sigma_n^2}} \\ &= \alpha \end{aligned} \tag{3.14}$$

With the superscript NP denoting the probability of false alarm using the Neyman-Pearson detector. γ^{NP} is solely determined by $p(z/H_0,T)$, resulting in an independence of the range for $P_{fa}(T)$.

Solving equation 3.14 for $\gamma^{NP}(T)$ results in:

$$\gamma^{NP}(T) = -T\sigma_n^2 \log(1-\alpha) \tag{3.15}$$

$P_{rej}^{NP}(T)$, $P_{miss}^{NP}(R,T)$ and $P_{det}^{NP}(R,T)$ are determined using equations 3.11, 3.12, 3.13 and 3.15, resulting in:

$$\begin{aligned} P_{rej}^{NP}(T) &= 1 - \alpha \\ P_{miss}^{NP}(R,T) &= 1 - e^{-log\Big(-T\sigma_n^2\log(1-\alpha)\big(1+SNR(R,T)\big)\Big)\frac{1}{SNR(R,T)}} \\ P_{det}^{NP}(R,T) &= 1 - P_{miss,R}^{NP}(T) \end{aligned} \tag{3.16}$$

It is emphasized that $P_{fa}(T)$, $P_{rej}^{NP}(T)$, $P_{miss}^{NP}(R,T)$ and $P_{det}^{NP}(R,T)$ all are monotone decreasing as function of T. Reflecting that increasing T will result in statistically better detector decisions.

The determination of γ^{NP} through equation 3.14 depends only on the measurement model of $p(z/H_0)$, and not on R, $P(H_0)$ and $P(H_1)$. An advantage of the Neyman-Pearson detector is that it can be implemented when no prior probabilities are available. Deciding that an object is present often triggers

a reaction from the radar user that drains resources. [12] states that these two reasons together make the Neyman-Pearson detector a popular detector choice for a wide range of applications.

The advantage of determining the threshold without taking into account the probabilities $P(H_0)$ and $P(H_1)$ becomes a disadvantage when $P(H_0)$ and $P(H_1)$ are available. Subsection 3.2.5 follows a popular detector framework that includes $P(H_0)$ and $P(H_1)$ in the process of determining γ.

3.2.5 Minimum Probability of Error

The minimum probability of error detector minimizes the probability that the detector makes an incorrect decision. The incorrect events are a miss and false alarm as defined in Section 3.2. The probability of an incorrect decision due to miss is the event that H_0 is accepted while the object is present, denoted by $P\Big(\big(L(z) < \gamma\big) \cap H_1/R,T\Big)$. The probability of making an incorrect decision due to a false alarm is the event that H_1 is accepted while the object is absent, denoted by $P\Big(\big(L(z) > \gamma\big) \cap H_0/R,T\Big)$. The minimum probability of error detector bases its decision on [11]:

$$\begin{aligned} P\Big(\big(L(z) < \gamma\big) \cap H_1/R,T\Big) &\underset{H_0}{\overset{H_1}{\gtrless}} P\Big(\big(L(z) > \gamma\big) \cap H_0/R,T\Big) \\ P_{miss}(R,T)P(H_1) &\underset{H_0}{\overset{H_1}{\gtrless}} P_{fa}(R,T)P(H_0) \end{aligned} \tag{3.17}$$

The threshold γ^{PE} that results in the minimum probability of error for a detector decision is $\gamma^{PE} = \frac{P(H_0)}{P(H_1)}$.

Choosing γ^{PE} as threshold in equations 3.10, 3.11, 3.12 and 3.13 results in:

$$\begin{aligned} P_{fa}^{PE}(R,T) &= e^{-log\left(\frac{P(H_0)}{P(H_1)}\left(1+SNR(R,T)\right)\right)\frac{SNR(R,T)+1}{SNR(R,T)}} \\ P_{rej}^{PE}(R,T) &= 1 - P_{fa}^{PE}(R,T) \\ P_{miss}^{PE}(R,T) &= 1 - e^{-log\left(\frac{P(H_0)}{P(H_1)}\left(1+SNR(R,T)\right)\right)\frac{1}{SNR(R,T)}} \\ P_{det}^{PE}(R,T) &= P_{miss}^{PE}(R,T) \end{aligned} \tag{3.18}$$

The threshold of $\frac{P(H_0)}{P(H_1)}$ for a minimum probability of error detector is a general result and is not limited to the specific choice of measurement models for H_0 and H_1. [11].

Choosing such a threshold value for γ enables the detector to adapt the threshold based on prior knowledge of $P(H_0)$ and $P(H_1)$.

For $P(H_0) = xP(H_1)$ the likelihood of a measurement generated by $p\big(z/H_1,R,T\big)$ must be a factor x higher than the likelihood of $p\big(z/H_0,T\big)$. For example, when $P(H_0) = 0.75$ and $P(H_1) = 1 - P(H_0) = 0.25$ require that the measurement is at least three times more likely to be generated by the object presence model than by the object absence model, for the detector to decide that an object is present.

Including prior knowledge $P(H_0)$ and $P(H_1)$ in detector decisions has the advantage of including more knowledge. A minimum probability of error detector is expected to make statistically the least number of errors. Where a Neyman-Pearson detector does not change the threshold as $P(H_1)$ changes, the minimum probability of error detector allows adaptation to a scenario by including $P(H_0)$ and $P(H_1)$ in the threshold. A minimum probability of error detector does not take into account the impact of a false alarm or a missed detection. The impact of false alarms and missed detection can have different consequences for a radar user depending on the radar application.

For example, within an autonomous vehicle system, missed detections or false alarms made by a collision avoidance radar have different consequences on the application level. A false alarm in short range might lead to unnecessarily braking, while missed detection might lead to collision. In such a case, it is likely that the autonomous car might favor relative more false alarms over more collisions. In contrast, a perimeter control radar that periodically scans a large area every few seconds might favor

relative more missed detections over false alarms. As a false alarm could trigger security responses, and a missed detection might lead to a delayed detection.

The above two scenarios give motivation that the negative effects of missed detections and false alarms differ per application. A minimum probability of error detector does not take into account the significance of the negative effects of either incorrect decision.

Another decision framework used in radar is the minimax approach. The minimax approach allows the user to specify the relative impact of a missed detection or false alarm. Section 3.2.7 does allow to take into account the negative effects of misses and false alarms by assigning costs to either event.

3.2.6 Minimax

The minimax detector minimizes the conditional risk of the detector decision with respect to the existence of the object. [13] Conditional risk for an object absence decision is defined as:

$$R_0(R,T) = C_{miss}P_{miss}(R,T) + C_{rej}P_{rej}(R,T) \tag{3.19}$$

And the conditional risk for an object presence decision is defined as:

$$R_1(R,T) = C_{fa}P_{fa}(R,T) + C_{det}P_{det}(R,T) \tag{3.20}$$

With C_{rej}, C_{fa}, C_{miss} and C_{det} are the negative relative impacts on the application level for correct rejection, false alarm, missed detection and correct detection for the detector decision regarding the presence of an object. Conditional risk is the risk associated with a detector decision without taking into account the probability of the hypothesis.

The minimax bases its decision on the following equation [13]:

$$\begin{aligned} R_0(R,T) &\underset{H_0}{\overset{H_1}{\gtrless}} R_1(R,T) \\ C_{rej}P_{rej}(R,T) + C_{miss}P_{miss}(R,T) &\underset{H_0}{\overset{H_1}{\gtrless}} C_{fa}P_{fa}(R,T) + C_{det}P_{det}(R,T) \end{aligned} \tag{3.21}$$

The assumption is made that $C_{rej} < C_{fa}$ and $C_{miss,R} < C_{det,R}$, which implies that a correct decision for a given hypothesis has less negative impact on the radar mission than an incorrect decision. The threshold for the minimax detector is $\gamma^{minimax} = \frac{C_{fa}-C_{rej}}{C_{miss}-C_{det}}$.

Choosing $\gamma^{minimax}$ as threshold in equations 3.10, 3.11, 3.12 and 3.13 results in:

$$\begin{aligned} P_{fa}^{minimax}(R,T) &= e^{-log\left(\frac{C_{fa}-C_{rej}}{C_{miss}-C_{det}}\left(1+SNR(R,T)\right)\right)\frac{SNR(R,T)+1}{SNR(R,T)}} \\ P_{rej}^{minimax}(R,T) &= 1 - P_{fa}^{minimax}(R,T) \\ P_{miss}^{minimax}(R,T) &= 1 - e^{-log\left(\frac{C_{fa}-C_{rej}}{C_{miss}-C_{det}}\left(1+SNR(R,T)\right)\right)\frac{1}{SNR(R,T)}} \\ P_{det}^{minimax}(R,T) &= 1 - P_{miss}^{minimax}(R,T) \end{aligned} \tag{3.22}$$

Using a detector based on equation 3.22 enables the radar to influence the probabilities of $P_{fa}^{minimax}(R,T)$ and $P_{miss}^{minimax}(R,T)$ by adjusting the values of C_{rej}, C_{fa}, C_{miss} and C_{det}.

Using the perimeter control radar example from Section 3.2.5, the user is more likely to assign relative higher costs to C_{fa} and C_{rej} compared to C_{det} and C_{miss}, allowing the detector to require stronger evidence for H_1 than for H_0 before deciding the presence of an object. Taking into account the costs of C_{rej}, C_{fa} and C_{miss} and C_{det} to set the decision threshold allows the detector to weigh the impact of the decision on the application level.

Subsection 3.2.7 considers a minimum Bayes risk detector, which combines the prior probability of an object being present and the costs of detector decisions.

3.2.7 Minimum Bayes risk

The minimum Bayes risk detector takes into account the prior knowledge $P(H_0)$ and $P(H_1)$ and the relative impact of decisions C_{rej}, C_{fa}, C_{miss} and C_{det} to determine the value of the detector threshold.

The cost of an event multiplied by the probability that such an event occurs is defined as the risk. The risk associated with an object absent decision is defined as:

$$R_0^{BR}(R,T) = C_{miss}P_{miss}(R,T)P(H_1) + C_{rej}P_{rej}(R,T)P(H_0) \tag{3.23}$$

And the risk associated with an object present decision is defined as:

$$R_1^{BR}(R,T) = C_{fa}P_{fa}(R,T)P(H_0) + C_{det}P_{det}(R,T)P(H_1) \tag{3.24}$$

The minimum Bayes risk detector decides H_0 or H_1 based on comparing the risk of either decision:

$$\begin{gathered} R_0^{BR}(R,T) \underset{H_0}{\overset{H_1}{\gtrless}} R_1^{BR}(R,T) \\ C_{miss}P_{miss}(R,T)P(H_1) + C_{rej}P_{rej}(R,T)P(H_0) \underset{H_0}{\overset{H_1}{\gtrless}} C_{fa}P_{fa}(R,T)P(H_0) + C_{det}P_{det}(R,T)P(H_1) \\ C_{miss,i}P_{miss,i}(R_i,T_i)P(H_{1,i}) + C_{fa,i}P_{fa,i}(R_i,T_i)P(H_{0,i}) \end{gathered} \tag{3.25}$$

The threshold for the minimum Bayes risk detector is $\gamma^{BR} = \frac{(C_{fa}-C_r)P(H_0)}{(C_m-C_d)P(H_1)}$. Choosing γ^{BR} as threshold in equations 3.10, 3.11, 3.12 and 3.13 results in:

$$\begin{aligned} P_{fa,R}^{BR}(R,T) &= e^{-log\left(\frac{(C_{fa}-C_r)P(H_0)}{(C_m-C_d)P(H_1)}\left(1+SNR(R,T)\right)\right)\frac{SNR(R,T)+1}{SNR(R,T)}} \\ P_{rej}^{BR}(R,T) &= 1 - P_{fa,R}^{BR}(R,T) \\ P_{miss}^{BR}(R,T) &= 1 - e^{-log\left(\frac{(C_{fa}-C_r)P(H_0)}{(C_m-C_d)P(H_1)}\left(1+SNR(R,T)\right)\right)\frac{1}{SNR(R,T)}} \\ P_{det}^{BR}(R,T) &= 1 - P_{miss}^{BR}(R,T) \end{aligned} \tag{3.26}$$

γ^{BR} has the advantage that it includes both the probabilities $P(H_0)$ and $P(H_1)$ and the costs C_{rej}, C_{fa}, C_{miss} and C_{det}, resulting in a minimized expected cost. In scenarios such as the autonomous car example from chapter 3.2.5, a minimum Bayes risk detector is able to trade off the risk between unnecessarily braking versus colliding by adjusting the ratio of $\frac{C_{miss}}{C_{fa}}$ and simultaneously taking into account the prior probability of an object being present, $P(H_1)$.

4 Formulating cost functions for a single object presence decision per scan direction

Formulating cost functions for a single object presence decision per scan direction This chapter considers a scenario with I_d object presence decisions, each in a different scan direction. The goal of this chapter is to present two optimization problems, which both provide a mathematical approach to distribute the available resource, the scan time budget, over the I_d scan directions. It formulates the general problem formulation at the system level in Section 4.1. The costs for individual decisions (tasks) are defined in Subsections 4.1.1, 4.1.3 and 4.1.4, assuming Neyman-Pearson, minimax and minimum Bayes risk detectors. Subsection 4.1.2 formulates both the cost for individual tasks and at the system level for a minimum probability of error detector. Section 4.2 compares the costs presented in Subsections 4.1.1, 4.1.2, 4.1.3 and 4.1.4 and provides arguments to continue with the cost formulation of the minimum Bayes Risk detector at task level, to formulate a cost function at the system level in Section 4.3.

4.1 The resource management problem formulation at the system level

Consider a radar manager that is tasked with dividing radar resources in order to provide the highest expected performance for a mission. The mission of the radar is to obtain the best, yet undefined, performance to decide the presence of objects. In total, there are I_d potential objects, each in different directions.

The radar uses scans to gather evidence on the presence of each object. Given that an object is absent, the measurement is generated by equation 3.2.1. Given that an object is present, the measurement is generated by equation 3.2.2.

As mentioned in Subsection 3.2.2, the expected evidence for the true hypotheses, provided by a measurement, increases as the scan time budget increases. The radar manager has a total scan time budget T to distribute in I_d directions. The i^{th} performance of each of the I_d object presence decisions is formulated as a task $t_i(T_i)$, defined in Subsections 4.1.1, 4.1.2, 4.1.3 and 4.1.4, with T_i the budget allocated to direction i. Given a total budget T, it must hold $T = \sum_{i=1}^{I_d} T_i$.

Within a radar, the detector is assigned to decide the presence of an object, aided by the likelihoods of both hypotheses, obtained through measurements. An incorrect detector decision on the presence of an object causes either a false alarm or a missed detection, both of which have a direct interpretation in a radar application context. Having a direct interpretation on the application level eases the task of a radar user in formulating for each task the relative significance of both missed detections and false alarms. For this reason, it is proposed to quantify the performance of each task based on the detector used.

The detectors used in radar are Neyman-Pearson, minimum probability of error, minimax, and minimum Bayes risk, the decision mechanism of each is formulated in chapter 3. The performance of each detector improves as the budget increases. This chapter demonstrates how an optimization problem can be formulated that includes a single cost function that combines all I_d task performances into a single cost function and uses an equality constraint to address the finite resource T available for the mission.

The proposed optimization problem structure is:

$$\begin{aligned} \underset{T_1,...,T_{I_d}}{\text{minimize}} \quad & f_{\text{system}}\left(t_1(R_1,T_1),...,t_{I_d}(R_{I_d},T_{I_d})\right) \\ \text{subject to} \quad & T = \sum_{i=1}^{I_d} T_i \\ & T_i \geq 0, \qquad i = 1,...,I_d \end{aligned} \tag{4.1}$$

With $f_{\text{system}}\left(t_1(R_1,T_1),...,t_{I_d}(R_{I_d},T_{I_d})\right)$ representing a cost function on the system level, that quantifies the global performance of all I_d decisions as a function of the scan time. Minimizing $f_{\text{system}}\left(t_1(R_1,T_1),...,t_{I_d}(R_{I_d},T_{I_d})\right)$ for $[T_1,...,T_{I_d}]$ results in the desired scan time distribution.

The minimization in equation 4.1 assumes that $f_{\text{system}}\left(t_1(R_1,T_1),...,t_{I_d}(R_{I_d},T_{I_d})\right)$ is a negative performance, cost. An alternative is to maximize $f_{\text{system}}\left(t_1(R_1,T_1),...,t_{I_d}(R_{I_d},T_{I_d})\right)$, using an utility interpretation. An overview of utility approaches for mission-driven resource allocation is given in [14].

To formulate $f_{\text{system}}\left(t_1(R_1,T_1),...,t_{I_d}(R_{I_d},T_{I_d})\right)$, the relative importance of each individual task is required. Each task is formulated as expected cost to have a single unifying interpretation at the system level. The significance of each task is formulated in Subsections 4.1.1, 4.1.2, 4.1.3 and 4.1.4 assuming Neyman-Pearson, minimum probability of error, minimax and minimum Bayes risk detectors, respectively.

4.1.1 Task cost using a Neyman-Pearson detector

The Neyman-Pearson detector is used when the radar user constrains the probability of a false alarm, notated $P^{NP}_{fa,\{i\}}$ for the i^{th} task, to a fixed value. The corresponding detector threshold $\gamma_i^{NP}(T_i)$ is fixed by the constraint of a predetermined probability of false alarm for a given budget T_i. Therefore, fixing a probability of false alarm implies a fixed $P^{NP}_{miss,\{i\}}(T_i,R)$, which is given by equation 3.16.

Allocating more budget to $t_i(T_i)$ only improves the monotonically decreasing function $P^{NP}_{miss,\{i\}}(R,T_i)$. Therefore, using a Neyman-Pearson detector results in a cost function at system level that makes a trade off between the probability of misses for different tasks.

The expected cost of the i^{th} task is:

$$t_i^{NP}(R_i,T_i) = C_{fa,i}P^{NP}_{fa,\{i\}}P(H_{0,i}) + C_{miss,i}P^{NP}_{miss,\{i\}}(R_i,T_i)P(H_{1,i}) \tag{4.2}$$

with $C_{fa,i}$ and $C_{miss,i}$ quantifying the significance of a false alarm and missed detection occurring for the i^{th} task, provided by the user.

Including prior knowledge of which of the hypotheses is true, $P(H_{0,i})$ and $P(H_{1,i})$ enables the system cost function to adjust the allocated budget depending on the uncertainty of the presence of an object. Including $C_{fa,i}$ and $C_{miss,i}$ enables the system cost function to adjust the allocated budget according to the significance of both events. Increasing the values of $C_{fa,i}$ and $C_{miss,i}$ relative to $C_{fa,j}$ and $C_{miss,j}$ with $i \neq j$, influences the cost function to increase T_i and decrease T_j. The interpretation of $t_i^{NP}(T_i)$ is the expected cost as a function of the budget T_i, having a fixed probability of false alarm.

The left term in equation 4.2 lacks a dependency on the budget variable T_i, and remains constant regardless of the value of T_i.

The resulting optimization problem is:

$$\begin{aligned} \underset{T_1,...,T_{I_d}}{\text{minimize}} \quad & f_{\text{system}}\left(t_1^{NP}(R_1,T_1),...,t_{I_d}^{NP}(R_{I_d},T_{I_d})\right) \\ \text{subject to} \quad & T = \sum_{i=1}^{I_d} T_i \\ & T_i \geq 0, \qquad i = 1,...,I_d \end{aligned} \tag{4.3}$$

with f_{system} yet undefined.

Within the current problem, a fixed budget T is assumed to be available for all I_d tasks combined. Within an MFR, the values $C_{fa,i}$ and $C_{miss,i}$ have additional meaning by impacting the total amount of budget T available for the I_d tasks, reducing the available budget for other radar functions.

Subsection 4.1.2 addresses how to quantify the significance of indvidiual tasks using a minimum probability of error detector.

4.1.2 Task and system cost using a minimum probability of error detector

The minimum probability of error detector is used when the radar user aims to minimize the probability of error for individual tasks regarding the presence of an object. Using this approach, the detector assigns equal costs to a missed detection and a false alarm.

The minimum probability of error for a single decision can be interpreted as the minimum probability of any error. This approach emphasizes how the minimum probability of error detector chooses the threshold such that the probability of any error is minimized. Extending this to multiple decisions leads to an interpretation of minimizing the probability that any error occurs. Defining the event that l out of I_d decisions are incorrect as E_l, the probability of any error is defined as:

$$P_{error,any}(R_1,...,R_{I_d},T_1,..,T_{I_d}) = \sum_{l=1}^{I_d} P\big(E_l(R_1,...,R_{I_d},T_1,..,T_{I_d})\big) \tag{4.4}$$

which can be reformulated by using $1 = P\big(E_0(R_1,...,R_{I_d},T_1,..,T_{I_d})\big) + \sum_{l=1}^{I_d} P\big(E_l(R_1,...,R_{I_d},T_1,..,T_{I_d})\big)$. Minimizing $\sum_{l=1}^{I_d} P\big(E_l(R_1,...,R_{I_d},T_1,..,T_{I_d})\big)$ is achieved by maximizing $P\big(E_0(R_1,...,R_{I_d},T_1,..,T_{I_d})\big)$, which is the probability that all I_d decisions are correct. This would result in an optimization problem of:

$$\begin{aligned} \underset{T_1,...,T_I}{\text{maximize}} \quad & P\big(E_0(R_1,...,R_{I_d},T_1,..,T_{I_d})\big) \\ \text{subject to} \quad & T = \sum_{i=1}^{I_d} T_i \\ & T_i \geq 0, \qquad i = 1,...,I_d \end{aligned} \tag{4.5}$$

By merging all the error probabilities of each task into a single event, the freedom of the user to express significance of the performance of individual tasks is eliminated. Multiplying $P_{error,any}$ with a cost coefficient can lead to an increase in the available budget T for object detection tasks in an MFR setting, but does not influence the relative budget distribution between tasks.

The alternative is to formulate the cost of individual tasks as expected cost. The cost for the i^{th} task is formulated as:

$$t_i^{PE}(R_i,T_i) = C_{fa,i}\big(P_{fa,\{i\}}^{PE}(R_i,T_i)P(H_{0,i}) + C_{miss,i}P_{miss,\{i\}}^{PE}(R_i,T_i)P(H_{1,i})\big) \tag{4.6}$$

Equation 4.6 is coherent with the minimum probability of error detector performance under the assumption that $C_{fa,i} = C_{miss,i}$. In the case of $C_{fa,i} = C_{miss,i}$, the absolute value of $C_{fa,i}$ is used to prioritize different tasks. Using a minimum probability of error detector with assigning $C_{fa,i} \neq C_{miss,i}$ in equation 4.6 loses the interpretation of the cost function to predict the expected cost of the detector decision.

Using equation 4.6 leads to the following optimization problem:

$$\begin{aligned} \underset{T_1,...,T_I}{\text{minimize}} \quad & f_{\text{system}}\big(t_1^{PE}(R_1,T_1),...,t_{I_d}^{PE}(R_{I_d},T_{I_d})\big) \\ \text{subject to} \quad & T = \sum_{i=1}^{I_d} T_i \\ & T_i \geq 0, \qquad i = 1,...,I_d \end{aligned} \tag{4.7}$$

with f_{system} yet undefined.

Subsection 4.1.3 addresses how to quantify the significance of individual tasks using a minimax detector which enables different cost coefficients defined for false alarms and missed detections.

4.1.3 Task cost using a minimax detector

The minimax detector is used when the user has provided costs coefficients for false alarms and missed detections, but there is no (reliable) prior information available regarding the presence of the object.

The cost for the i^{th} task is formulated as:

$$t_i^{minimax}(R_i, T_i) = C_{fa,i} P_{fa,\{i\}}^{minimax}(R_i, T_i) P(H_{0,i}) + C_{miss,i} P_{miss,\{i\}}^{minimax}(R_i, T_i) P(H_{1,i}) \tag{4.8}$$

Equation 4.8 is coherent with the minimax detector performance under the assumption that $P(H_{0,i}) = P(H_{1,i})$. For a scenario with $P(H_{0,i}) \neq P(H_{1,i})$, equation 4.8 does not predict the expected cost of the detector. For the detector itself, only the ratio between $C_{fa,i}$ and $C_{miss,i}$ is important, while for the cost function at the system level, the magnitude of both $C_{fa,i}$ and $C_{miss,i}$ relative to $C_{fa,j}$ and $C_{miss,j}$ for $i \neq j$ has the additional meaning of expressing the relative importance of individual tasks at the system level.

Using equation 4.8 leads to the following optimization problem:

$$\begin{aligned} \underset{T_1,...,T_{I_d}}{\text{minimize}} \quad & f_{\text{system}}\left(t_1^{minimax}(R_1, T_1), ..., t_{I_d}^{minimax}(R_{I_d}, T_{I_d})\right) \\ \text{subject to} \quad & T = \sum_{i=1}^{I_d} T_i \\ & T_i \geq 0, \qquad i = 1, ..., I_{I_d} \end{aligned} \tag{4.9}$$

Subsection 4.1.4 addresses how to quantify the significance of individual tasks using a minimum Bayes risk detector which enables different cost coefficients defined for false alarms and missed detections while taking into account prior information $P(H_{1,i})$.

4.1.4 Task cost using a minimum Bayes risk detector

The minimum Bayes risk detector both takes into account prior knowledge $P(H_{1,i})$ and the costs associated with false alarms and missed detections, $C_{fa,i}$ and $C_{miss,i}$, respectively. The expected cost of the i^{th} task is formulated as:

$$t_i^{BR}(R_i, T_i) = C_{fa,i} P_{fa,\{i\}}^{BR}(R_i, T_i) P(H_{0,i}) + C_{miss,i} P_{miss,\{i\}}^{BR}(R_i, T_i) P(H_{1,i}) \tag{4.10}$$

$t_i^{BR}(R_i, T_i)$ represents the total expected risk. $C_{fa,i}$ and $C_{miss,i}$ enable the user to quantify the relative significance on the system level of the i^{th} task compared to the other tasks. Including $P(H_{1,i})$ allows the radar to focus its budget on objects with a high uncertainty of the presence of the object.

Using equation 4.10 results in the following optimization problem:

$$\begin{aligned} \underset{T_1,...,T_{I_d}}{\text{minimize}} \quad & f_{\text{system}}\left(t_1^{BR}(R_1, T_1), ..., t_{I_d}^{BR}(R_{I_d}, T_{I_d})\right) \\ \text{subject to} \quad & T = \sum_{i=1}^{I_d} T_i \\ & T_i \geq 0, \qquad i = 1, ..., I_d \end{aligned} \tag{4.11}$$

In the minimum probability of error approach, a direct extension to system level was possible by combining multiple events (error decisions of individual tasks) into one event at the system level as given in equation 4.5. The minimum Bayes risk detector does not allow such an interpretation due to the dimension of risk being (expected) cost instead of probability.

Section 4.2 compares $t_i^{NP}(R_i, T_i)$, $t_i^{PE}(R_i, T_i)$, $t_i^{minimax}(R_i, T_i)$ and $t_i^{BR}(R_i, T_i)$.

4.2 Comparison

The type of detector directly influences the choice of $t_i(R_i, T_i)$ as demonstrated in Subsections 4.1.1, 4.1.2, 4.1.3 and 4.1.4. This Section motivates the proposal to choose the quantification of cost for an individual task using $t_i^{BR}(R_i, T_i)$ as defined in equation 4.10 to achieve the research aims formulated in the introduction.

Using a Neyman-Pearson detector resulted in $t_i^{NP}(T_i)$ from equation 4.2 as the cost quantification of an individual task. In the scenario where the user requires a fixed probability of false alarm, $t_i^{NP}(T_i)$ is proposed to represent the cost of individual tasks at the system level.

Using a minimum probability of error detector resulted in $t_i^{PE}(R_i, T_i)$ from equation 4.6 as the cost quantification of an individual task. $t_i^{PE}(R_i, T_i)$ only has the interpretation of the expected cost of the detector decision when $C_{miss,i} = C_{fa,i}$.

Using a minimax detector resulted in $t_i^{minimax}(R_i, T_i)$ from equation 4.8 as the cost quantification of an individual task. $t_i^{minimax}(R_i, T_i)$ only has the interpretation of the expected cost of the detector decision when $P(H_{i,1}) = P(H_{i,0})$.

Using a minimum Bayes risk detector resulted in $t_i^{BR}(R_i, T_i)$ from equation 4.10 as the cost quantification of an individual task. $t_i^{BR}(R_i, T_i)$ has the interpretation of the expected cost of the detector decision for all values of $P(H_{i,1})$, $C_{miss,i}$ and $C_{fa,i}$.

$t_i^{BR}(R_i, T_i)$ is preferred over $t_i^{PE}(R_i, T_i)$ and $t_i^{minimax}(R_i, T_i)$ as $t_i^{BR}(R_i, T_i)$ retains the interpretation of the expected cost of the detector decision for a larger domain of $P(H_{i,1})$, $C_{miss,i}$ and $C_{fa,i}$.

The rest of this thesis assumes that the user does not require a fixed probability of false alarm. Under this assumption, it is recommended that the significance of individual tasks is formulated as $t_i^{BR}(T_i)$ from equation 4.10.

Section 4.3 formulates a cost function at the system level based on formulating individual tasks using $t_i^{BR}(R_i, T_i)$.

4.3 Formulating a cost function at the system level

This section formulates $f_{\text{system}}\left(t_1^{BR}(R_1, T_1), ..., t_{I_d}^{BR}(R_{I_d}, T_{I_d})\right)$ in equation 4.11.

In order to maintain the meaning of $t_i^{BR}(T_i)$, $f_{\text{system}}\left(t_1^{BR}(R_1, T_1), ..., t_{I_d}^{BR}(R_{I_d}, T_{I_d})\right)$ must preserve the dimension of risk. Two implementations of $f_{\text{system}}\left(t_1^{BR}(R_1, T_1), ..., t_{I_d}^{BR}(R_{I_d}, T_{I_d})\right)$ are proposed.

The first proposed implementation of $f_{\text{system}}\left(t_1^{BR}(R_1, T_1), ..., t_{I_d}^{BR}(R_{I_d}, T_{I_d})\right)$ is to minimize the expected risk at the system level. Minimizing the expected risk at the system level is obtained by summing the expected risk of each individual task. This results in the following optimization problem:

$$\begin{aligned} \underset{T_1,...,T_{I_d}}{\text{minimize}} \quad & \sum_{i=1}^{I_d} t_i^{BR}(R_i, T_i) \\ \text{subject to} \quad & T = \sum_{i=1}^{I_d} T_i \\ & T_i \geq 0, \qquad i = 1, ..., I_d \end{aligned} \tag{4.12}$$

In the special case of $I_d = 1$, the trivial solution of $T = T_1$ results in equal cost functions at the system level and at task level.

Solving the optimization problem in equation 4.12 for $I_d > 1$ results in the distribution of T that is expected to minimize the total risk of all I_d tasks combined.

The second proposed implementation of $f_{\text{system}}\left(t_1^{BR}(R_1, T_1), ..., t_{I_d}^{BR}(R_{I_d}, T_{I_d})\right)$ is to minimize the maximum risk of any individual task. This results in the following optimization problem:

$$\begin{aligned} \underset{T_1,...,T_{I_d}}{\text{minimize}} \quad & \max\{t_1^{BR}(R_1, T_1), ..., t_{I_d}^{BR}(R_{I_d}, T_{I_d})\} \\ \text{subject to} \quad & T = \sum_{i=1}^{I_d} T_i \\ & T_i \geq 0, \qquad i = 1, ..., I_d \end{aligned} \tag{4.13}$$

The optimization problem in equation 4.13 selects the distribution of T such that the maximum risk of all I_d tasks is minimized.

5 Formulating cost functions for generalized scenarios

This chapter generalizes the scenario in Section 4 and redefines the individual tasks and cost function at the system level accordingly. Section 5.1 generalizes each scan direction to M object presence decisions. Section 5.2 extends the scenario by considering previous measurements. Section 5.3 extends the scenario by introducing a birth-death process for each potential object.

5.1 Extending each task to M object presence decisions

This section extends the scenario from Chapter 4 by extending each individual task to decide the presence of multiple objects in the same direction, each at a different range.

The range in each task is discretized in J cells, motivated by the requirement of a Bayes risk detector to have a prior probability instead of a prior probability density. The range discretization requires the detector to make J decisions about the presence of an object per task. To simplify the notation, the j^{th} range cell is denoted by subscript j. For example, the probability that an object exists in the i^{th} direction at the j^{th} range cell is notated as $P(H_{1,\{i,j\}})$.

The assumption is made that the probability of object presence in each cell is independent of the presence of objects in other cells, and a maximum of one object is simultaneously present in each cell.

Having J different decisions to make per task, the user can provide J different cost coefficients for misses and false alarms per task. The cost of a miss and false alarm occurring in the i^{th} direction at the j^{th} range cell are notated as $C_{miss,\{i,j\}}$ and $C_{fa,\{i,j\}}$ respectively. Allowing the radar user to provide costs per individual range cell and direction enables the radar user to assign spatial zones that are of relative high or low importance. A relatively large $C_{miss\{i,j\}}$ and $C_{fa\{i,j\}}$ compared to $C_{miss\{i,m\}}$ and $C_{fa\{i,m\}}$ would result in a higher contribution of the cost function at the system level caused by the j^{th} range cell compared to the m^{th} range cell.

As explained in Chapter 3, both the probability of false alarm and missed detection for a minimum Bayes risk detector depend on the range caused by $SNR \propto \frac{1}{R^4}$. Using a similar notation, the probability of false alarms and missed detections for the i^{th} direction at the j^{th} range cell are defined as $P^{BR}_{fa,\{i,j\}}(T_i)$ and $P^{BR}_{miss,\{i,j\}}(T_i)$ respectively.

The cost of a single range cell is now defined as:

$$t'^{BR}_{i,j}(T_i) = C_{fa,\{i,j\}} P^{BR}_{fa,\{i,j\}}(T_i) P(H_{0,\{i,j\}}) + C_{miss,\{i,j\}} \mathrm{P}^{BR}_{miss,\{i,j\}}(T_i) P(H_{1,\{i,j\}}) \tag{5.1}$$

Each cell in the i^{th} direction depends on the same budget T_i, resulting in an optimization problem that still has I_d different budget variables to optimize. It is proposed to redefine the i^{th} task as the expected total risk in the i^{th} direction:

$$t'^{\,BR}_{i,j}(T_i) = \sum_{j=1}^{J} t'^{\,BR}_{i,j}(T_i) \tag{5.2}$$

Using the definition of each task as in equation 5.2 causes the cost on task level to preserve the costs of individual cells. Rather than defining the task as $t'^{BR}_{i}(T_i) = max\{t'^{\,BR}_{i,1}(T_1), ..., t'^{\,BR}_{i,J}(T_J)\}$, which

reduces the cost of all cells to a single cell on the task level, thus losing the meaning of all but a single cell within each scan direction.

Using the redefinition of the i^{th} task as in equation 5.2, the optimization problem for the cost function at the system level that minimizes the total expected risk is:

$$\begin{aligned} \underset{T_1,...,T_{I_d}}{\text{minimize}} \quad & \sum_{i=1}^{I_d} {t'_{i,j}}^{BR}(T_i) \\ \text{subject to} \quad & T = \sum_{i=1}^{I_d} T_i \\ & T_i \geq 0, \qquad i = 1, ..., I_d \end{aligned} \tag{5.3}$$

The optimization problem formulated in equation 5.3 is a generalized version of 4.12. Equation 5.3 is equal to equation 4.12 when $J = 1$.

Using the redefinition of the i^{th} task as in equation 5.2, the optimization problem for the cost function at the system level that minimizes the maximum expected risk of any individual task is:

$$\begin{aligned} \underset{T_1,...,T_{I_d}}{\text{minimize}} \quad & \max\{{t'_1}^{BR}(T_1), ..., {t'_{I_d}}^{BR}(T_{I_d})\} \\ \text{subject to} \quad & T = \sum_{i=1}^{I_d} T_i \\ & T_i \geq 0, \qquad i = 1, ..., I_d \end{aligned} \tag{5.4}$$

The optimization problem in equation 5.4 is a generalization of equation 4.12. Both equations are equal under the condition that $J = 1$.

This extension demonstrated that the cost function at the system level can remain unchanged by redefining the definition of individual tasks. Section 5.2 extends the current extension by including previous measurements to update the prior information.

5.2 Sequential scans

The extension of this section is to perform multiple scans. Using multiple scans allows investigation of the change of budget allocation as the number of scans increases.

Cells at short range have a relative higher SNR due to $SNR \propto \frac{1}{R^4}$. A high SNR will result in measurements that are more likely to converge the probability of the true hypothesis to 1. The Bayes risk detector threshold takes into account this probability and adjusts the detector, resulting in a significant reduction in the risk for cells at short range.

Previous measurements update the probability of object presence. The posterior probability after a measurement is obtained through Bayes theorem.[15] Defining the k^{th} scan as the scan that is performed in the time interval $[(k-1)T,\ kT]$, notated as T^k. The set of the first k time intervals is notated as $T^{1:k}$.

The measurement in the k^{th} scan in the i^{th} direction at the j^{th} range cell is defined as, $z_{\{i,j\}}(T_i^k)$, with a simplified notation of $z_{\{i,j\}}^k$. The set of the first k measurements given the allocated budgets $T_i^{1:k}$ is defined as $Z_{\{i,j\}}(T_i^{1:k})$ with a simplified notation of $Z_{\{i,j\}}^k$.

Using the notation above, the updated posterior for the presence of the object at time index k at cell $\{i, j\}$, given prior knowledge, is given as:

$$P(H_{1,\{i,j\}}/Z_{\{i,j\}}^k) = \frac{p(z_{\{i,j\}}^k/H_{1,\{i,j\}})P(H_{1,\{i,j\}}/Z_{\{i,j\}}^{k-1})}{p(z_{\{i,j\}}^k/H_{0,\{i,j\}})P(H_{0,\{i,j\}}/Z_{\{i,j\}}^{k-1}) + p(z_{\{i,j\}}^k/H_{1,\{i,j\}})P(H_{1,\{i,j\}}/Z_{\{i,j\}}^{k-1})} \tag{5.5}$$

With $P(H_{1,\{i,j\}}/Z^k_{\{i,j\}})$ the posterior probability of the presence of an object after k measurements. $p(z^k_{\{i,j\}}/H_{0,\{i,j\}})$ and $p(z^k_{\{i,j\}}/H_{1,\{i,j\}})$ are the likelihoods of the measurement conditioned on the presence or absence of the object. $P(H_{0,\{i,j\}}/Z^{k-1}_{\{i,j\}})$ and $P(H_{1,\{i,j\}}/Z^{k-1}_{\{i,j\}})$ are the prior probability of the absence or presence of the object at time index k.

After each scan, the probability of the presence of the object is updated considering that each measurement provides evidence for both hypothesis. The relative difference in the evidence for both hypotheses determines the posterior probability.

The cost of an individual cell is now defined as:

$$t''^{BR,k}_{i,j}(T^k_i) = C^k_{fa,\{i,j\}} P^{BR}_{fa,\{i,j\}}(T^k_i) P(H_{0,\{i,j\}}/Z^{k-1}_{\{i,j\}}) + C^k_{miss,\{i,j\}} \mathrm{P}^{BR}_{miss,\{i,j\}}(T^k_i) P(H_{1,\{i,j\}}/Z^{k-1}_{\{i,j\}}) \tag{5.6}$$

Which can be used to define the task performance as:

$$t''^{BR,k}_{i}(T^k_i) = \sum_{j=1}^{J} t''^{BR,k}_{i,j}(T^k_i) \tag{5.7}$$

Resulting in an optimization problem that minimizes the expected risk as:

$$\begin{aligned} \underset{T^k_1,\dots,T^k_{I_d}}{\text{minimize}} \quad & \sum_{i=1}^{I_d} t''^{BR,k}_{i}(T^k_i) \\ \text{subject to} \quad & T^k = \sum_{i=1}^{I_d} T^k_i \\ & T^k_i \geq 0, \qquad i = 1, \dots, I_d \end{aligned} \tag{5.8}$$

And the optimization problem that minimizes the maximum expected risk of individual tasks as:

$$\begin{aligned} \underset{T^k_1,\dots,T^k_{I_d}}{\text{minimize}} \quad & \max\{t''^{BR,k}_{1}(T^k_1), \dots, t''^{\,BR,k}_{I_d}(T^k_{I_d})\} \\ \text{subject to} \quad & T^k = \sum_{i=1}^{I_d} T^k_i \\ & T^k_i \geq 0, \qquad i = 1, \dots, I_d \end{aligned} \tag{5.9}$$

Both equations 5.8 and 5.9 take into account previous measurements. The optimization problems in equations 5.3 and 5.4 can be seen as a special case of $k = 1$.

The current extension is a static scenario with respect to the presence of an object within a cell. The magnitudes of $\sum_{j=1}^{J} t''^{BR,k}_{i,j}(T^k_i)$ and $\max\{t''^{BR,k}_{1}(T^k_1), t''^{BR,k}_{I}(T^k_I)\}$ will decrease as k increases. Theoretically, as $\lim_{k\to\infty}$ both cost function go to zero.

In practice, a scenario changes over time. Section 5.3 introduces a birth-death process that results in the presence of an object that changes over time.

5.3 Birth-death Markov process

This section introduces birth-death processes with respect to the presence of an object.

A birth is the appearance of a new object in a cell provided that the object was previously absent. This event is modeled by a probability $P^k_{birth\{i,j\}}$, which represents the probability that an object is born after the k^{th} and before the $(k+1)^{th}$ scan.

A death is the disappearance of an existing object in a cell. This event is modeled by a probability $P^k_{death\{i,j\}}$, which represents the probability that an object disappears after the k^{th} and before the $(k+1)^{th}$ scan.

The extension of a birth-death process enables to investigate the effect a changing object presence over time has on the budget allocation, while fitting in the narrative of having a maximum of one object per cell. The difference in budget allocation between the extension of Section 5.2 and this section will illustrate the effect of a changing object presence over time. As the number of scans increases, this difference is expected to increase as the effect of prior knowledge $P(H_{1,\{i,j\}})$ becomes less significant over time for non-zero $P^k_{birth\{i,j\}}$ and $P^k_{death\{i,j\}}$.

The main difference of this extension is the time dependency of the presence of an object. The event of an object existing at time index k is now formulated as $H^k_{1,\{i,j\}}$, with the superscript k emphasizing the time dependency of the presence of the object.

Given the posterior at time index k-1, $P(H^{k-1}_{1,\{i,j\}}/Z^{k-1}_{\{i,j\}})$,the prior probability of object presence for time index k is given as [16]:

$$P(H^k_{1,\{i,j\}}/Z^{k-1}_{\{i,j\}}) = P^k_{birth\{i,j\}}P(H^{k-1}_{0,\{i,j\}}/Z^{k-1}_{\{i,j\}}) + (1 - P^k_{death\{i,j\}})P(H^{k-1}_{1,\{i,j\}}/Z^{k-1}_{\{i,j\}}) \tag{5.10}$$

Equation 5.10 emphasizes the difference between the posterior at time index $k-1$ and the posterior at time index k.

The introduction of a birth-death process also allows a method to calculate the prior $P(H^0_{1,\{i,j\}})$. Given that before the radar starts its mission at time index $k = 0$ there are no measurements performed, the prior is entirely determined by the birth-death process. Using zero budget allocation in any negative time index up to $k = 0$, a prior is found by recursively evaluating equation 5.10.

Modeling the birth and death mechanism as a Markov process results, using the definition of the probability of object survival as $P^k_{survival\{i,j\}} = 1 - P^k_{death\{i,j\}}$, in:

$$\begin{bmatrix} P(H^{-n+1}_{1,\{i,j\}}) \\ P(H^{-n+1}_{0,\{i,j\}}) \end{bmatrix} = \begin{bmatrix} P^{-n}_{survival\{i,j\}} & P^{-n}_{birth\{i,j\}} \\ P^{-n}_{death\{i,j\}} & 1 - P^{-n}_{birth\{i,j\}} \end{bmatrix} \begin{bmatrix} P(H^{-n}_{1,\{i,j\}}) \\ P(H^{-n}_{0,\{i,j\}}) \end{bmatrix} \tag{5.11}$$

Under the assumption of constant probability of birth and death, a prior can be found by:

$$\begin{bmatrix} P(H^0_{1,\{i,j\}}) \\ P(H^0_{0,\{i,j\}}) \end{bmatrix} = \lim_{n\to\infty} \left(\begin{bmatrix} P_{survival\{i,j\}} & P_{birth\{i,j\}} \\ P_{death\{i,j\}} & 1 - P_{birth\{i,j\}} \end{bmatrix} \right)^n \begin{bmatrix} P(H^{-n}_{1,\{i,j\}}) \\ P(H^{-n}_{0,\{i,j\}}) \end{bmatrix} \tag{5.12}$$

The matrix can be decomposed into its Eigenvalue decomposition with Eigenvalues $\lambda_1 = 1$ and $\lambda_2 = 1 - P_{birth\{i,j\}} - P_{death\{i,j\}}$:

$$\begin{aligned} &\lim_{n\to\infty} \left(\begin{bmatrix} P_{survival\{i,j\}} & P_{birth\{i,j\}} \\ P_{death\{i,j\}} & 1 - P_{birth\{i,j\}} \end{bmatrix} \right)^n \\ &= \lim_{n\to\infty} \begin{bmatrix} P_{birth,\{i,j\}} & 1 \\ P_{death,\{i,j\}} & -1 \end{bmatrix} \begin{bmatrix} 1^n & 0 \\ 0 & (1 - P_{birth,\{i,j\}} - P_{death,\{i,j\}})^n \end{bmatrix} \frac{1}{P_{birth,\{i,j\}} + P_{death,\{i,j\}}} \begin{bmatrix} 1 & 1 \\ P_{death,\{i,j\}} & -P_{birth,\{i,j\}} \end{bmatrix} \end{aligned} \tag{5.13}$$

Assuming $0 < |P_{birth\{i,j\}}| < 1$ and $0 < |P_{death\{i,j\}}| < 1$ results in λ_2 to go to zero as n approaches infinity, resulting in a limiting state of:

$$\begin{aligned} \begin{bmatrix} P(H^0_{1,\{i,j\}}) \\ P(H^0_{0,\{i,j\}}) \end{bmatrix} &= \lim_{n\to\infty} \left(\begin{bmatrix} P_{survival\{i,j\}} & P_{birth\{i,j\}} \\ P_{death\{i,j\}} & 1 - P_{birth\{i,j\}} \end{bmatrix} \right)^n \begin{bmatrix} P(H^{-n}_{1,\{i,j\}}) \\ P(H^{-n}_{0,\{i,j\}}) \end{bmatrix} \\ &= \begin{bmatrix} \frac{P_{death\{i,j\}}}{P_{birth\{i,j\}} + P_{death\{i,j\}}} \\ \frac{P_{birth\{i,j\}}}{P_{birth\{i,j\}} + P_{death\{i,j\}}} \end{bmatrix} \end{aligned} \tag{5.14}$$

The prior at time index k entirely based on $P_{birth\{i,j\}}$ and $P_{death\{i,j\}}$ given by equation 5.14 can be reasoned. Given that an object is absent, it is expected that it requires $\frac{1}{P_{birth\{i,j\}}}$ time intervals for

an object to be born. This newborn object is expected to live $\frac{1}{P_{death\{i,j\}}}$ time intervals before it dies, completing the cycle of birth and death. The fraction of the intervals that the object is alive is $\frac{\frac{1}{P_{death\{i,j\}}}}{\frac{1}{P_{death\{i,j\}}}+\frac{1}{P_{birth\{i,j\}}}} = \frac{P_{birth\{i,j\}}}{P_{birth\{i,j\}}+P_{death\{i,j\}}}$.

The cost of a cell is now defined as:

$$t_{i,j}^{'''BR,k}(T_i^k) = C_{fa,\{i,j\}}^k P_{fa,\{i,j\}}^{BR}(T_i^k) P(H_{0,\{i,j\}}^k / Z_{\{i,j\}}^{k-1}) + C_{miss,\{i,j\}}^k \mathrm{P}_{miss,\{i,j\}}^{BR}(T_i^k) P(H_{1,\{i,j\}}^k / Z_{\{i,j\}}^{k-1}) \quad (5.15)$$

with the priors $P(H_{0,\{i,j\}}^k / Z_{\{i,j\}}^{k-1})$ and $P(H_{1,\{i,j\}}^k / Z_{\{i,j\}}^{k-1})$ obtained through applying equation 5.10 using the posterior at time index $k-1$.

The i^{th} task is now defined as:

$$t_i^{'''BR,k}(T_i^k) = \sum_{j=1}^{J} t_{i,j}^{'''BR,k}(T_i^k) \quad (5.16)$$

The resulting optimization problem for minimizing the total expected risk is:

$$\begin{aligned} \underset{T_1^k,\dots,T_{I_d}^k}{\text{minimize}} \quad & \sum_{i=1}^{I_d} t_i^{'''BR,k}(T_i^k) \\ \text{subject to} \quad & T^k = \sum_{i=1}^{I_d} T_i^k \\ & T_i^k \geq 0, \qquad i = 1, \dots, I_d \end{aligned} \quad (5.17)$$

Similarly, the optimization problem for minimizing the maximum expected risk of an individual task is:

$$\begin{aligned} \underset{T_1^k,\dots,T_{I_d}^k}{\text{minimize}} \quad & \max\{t_1^{'''BR,k}(T_1^k), \dots, t_{I_d}^{'''BR,k}(T_I^k)\} \\ \text{subject to} \quad & T^k = \sum_{i=1}^{I_d} T_i^k \\ & T_i^k \geq 0, \qquad i = 1, \dots, I_d \end{aligned} \quad (5.18)$$

Both optimization problems take into account a birth and death probability when predicting the prior of the next scan, which is abstracted by $t_i^{'''BR,k}(T_i^k)$. f_{system} as function of the tasks remains unchanged for both approaches. The adjustment of the cost function is done by redefining individual tasks.

The optimization problems in equations 5.17 and 5.18 are a generalization of the optimization problems in equations 5.8 and 5.9. When $P_{birth\{i,j\}} = 0$ and $P_{death\{i,j\}} = 0$ for $i \in [1, \dots, I_d]$ and $j \in [1, \dots, J]$, equation 5.17 converges to 5.8 and equation 5.18 converges to 5.9.

6 Simulations and Results

This chapter simulates the scenarios in Chapters 4 and 5 to examine the allocation of the scan time budget by solving the corresponding optimization problems using the *Sum* and *Max* methods. The *Sum* method refers to the cost functions that allocate the budget based on the minimization of the sum of the expected risk of the tasks. The *Max* method refers to the cost functions that allocate the scan time budget based on the minimization of the maximum expected risk of the tasks. The simulations demonstrate the adaptability of both the *Sum* and *Max* methods to adjust the allocation of the scan time budget depending on the specific scenario. In each scenario, a third allocation of the scan time budget is used, the *Uniform* method, which uniformly distributes the budget over all tasks. The *Uniform* method represents the allocation of the scan time budget in the absence of a cost function.

Table 6.1 gives a high-level overview of the scenarios considered in this chapter. Section 6.1 considers a scenario as formulated in Section 4.1, where the radar has to distribute the scan time budget over two tasks, each consisting of a single range cell, for a single measurement. The *Sum* and *Max* methods in this scenario allocate the scan time budget by solving equations 4.12 and 4.13. This scenario is simulated for two different available scan time budget quantities, highlighting the effect of the magnitude of T.

Section 6.2 considers a scenario as formulated in Section 5.1. This scenario extends the previous scenario by extending each task to 991 range cells. The *Sum* and *Max* methods now distribute the scan time budget over the two tasks by solving equations 5.3 and 5.4.

Subsection 6.3.1 considers the scenario as formulated in Section 5.2. The scenario extends the previous scenario by extending the number of measurements to 32. The *Sum* and *Max* methods now distribute the scan time budget over the two tasks by solving equations 5.8 and 5.9.

Subsection 6.3.2 considers the scenario as formulated in Section 5.3. The scenario extends the previous scenario by including a nonzero probability of the birth and death of the object. In addition, the number of scans is increased from 32 to 64 to better visualize the effect a birth-death process has on the allocation of the scan time budget. The *Sum* and *Max* methods now distribute the scan time budget over the two tasks by solving equations 5.17 and 5.18.

Section 6.4 considers the scenario as formulated in Section 5.3. The scenario extends the previous scenario by increasing the number of tasks from two to three. The *Sum* and *Max* methods still distribute the scan time budget over the two tasks by solving equations 5.17 and 5.18.

Section	Tasks	Range cells per task	Scans	Birth/Death	*Sum* method	*Max* method
6.1	2	1	1	×	Eq 4.12	Eq 4.13
6.2	2	991	1	×	Eq 5.3	Eq 5.4
6.3.1	2	991	32	×	Eq 5.8	Eq 5.9
6.3.2	2	991	64	✓	Eq 5.17	Eq 5.18
6.4	3	991	48	✓	Eq 5.17	Eq 5.18

Table 6.1: High-level overview of scenarios

Each scenario uses a table such as Table 6.2 to present the chosen object parameters.

Task	$P(H_{1,x})$	$C_{miss,x}$	$C_{fa,x}$	$SNR(T,R)$	$P_{birth,x}$	$P_{death,x}$

Table 6.2: Object parameters table

The meaning of each column in Table 6.2 is

- Task: Scan direction that contain cells that require an object presence decision
- $P(H_{1,x})$: The prior probability that an object is present at the cell at position x
- $C_{miss,x}$: The cost of a missed detection at the cell at position x
- $C_{fa,x}$: The cost of a false alarm at the cell at position x
- $SNR(R,T)$: The SNR at range R having the entire scan time budget T allocated to the considered task
- $P_{birth,x}$: The probability of the birth of an object at position x
- $P_{death,x}$: The probability of death of an object at position x

The performance of an individual simulation is measured by transforming the risk of the *Sum*, *Max*, and *Uniform* methods into achieved cost caused by missed detections and false alarms based on simulated detector decisions.

Sections 6.1, 6.2, 6.3.1, 6.3.2 and 6.4 average the performance over 10000 simulations runs. Each individual simulation run has randomized object presence in each cell with probability equal to the prior probability $P(H_{1,x})$.

6.1 One decision per task

This Section simulates a scenario with two tasks with each a single range cell, for a single scan, as is shown in Table 6.3. The *Sum* and *Max* methods distribute the scan time budget solving equations 4.12 and 4.13. Two sets of object parameters are chosen, which differ in the magnitude of available scan time budget only, resulting in different $SNR(R,T)$. These two scenarios are compared to illustrate the effect the relative scan time budget has on the solutions of equations 4.12 and 4.13.

Tasks	Range cells per task	Scans	Birth/Death	Optimization Sum	Optimization Max
2	1	1	×	Eq 4.12	Eq 4.13

Table 6.3: Simulation parameters

The object parameters for scenario 1A are presented in Table 6.4. Both prior probabilities of the presence of the object are 0.5, representing the maximum uncertainty of the presence. $C_{miss} = C_{fa}$ for both tasks, with the first task having twice the cost compared to the second task. The double cost of false alarms and missed detections for task one compared to task two is chosen to emphasize the effect of the choice of the cost coefficients. Allocating the entire scan time budget to a single task results in a SNR of 10 for either task.

The object parameters for scenario 1B are presented in Table 6.5. The difference between scenario 1A and 1B is the maximum achievable SNR for a single task. For scenario 1B the maximum achievable SNR is 1 for either task.

Task	$P(H_1)$	C_{miss}	C_{fa}	$SNR(T)$	P_{birth}	P_{death}
1	0.5	2	2	10	0	0
2	0.5	1	1	10	0	0

Table 6.4: Object parameters scenario 1A

Task	$P(H_1)$	C_{miss}	C_{fa}	$SNR(T)$	P_{birth}	P_{death}
1	0.5	2	2	1	0	0
2	0.5	1	1	1	0	0

Table 6.5: Object parameters scenario 1B

The figure on the left in Figure 6.1 illustrates the risk per task as a function of the percentage of the scan time budget assigned to task 1 for scenario 1A. The expected risk for zero allocated scan time to a task is determined by $\min\Big(C_{miss}P(H_1), C_{fa}(1-P(H_1))\Big)$ using the values in Tables 6.4 and 6.5.

Increasing T_1 results in a decrease in risk for task 1 and an increase in risk for task 2, illustrating the trade-off of task performances that the cost function makes. The risks of both tasks are equal in magnitude at $T_1 = 0.822T$.

The figure on the right in Figure 6.1 illustrates the derivative of the risk of both tasks with respect to the scan time budget allocated to task 1 for scenario 1A, with the derivative of task 2 multiplied by -1 for illustration purposes. The derivatives of both tasks are equal at $T_1 = 0.645T$.

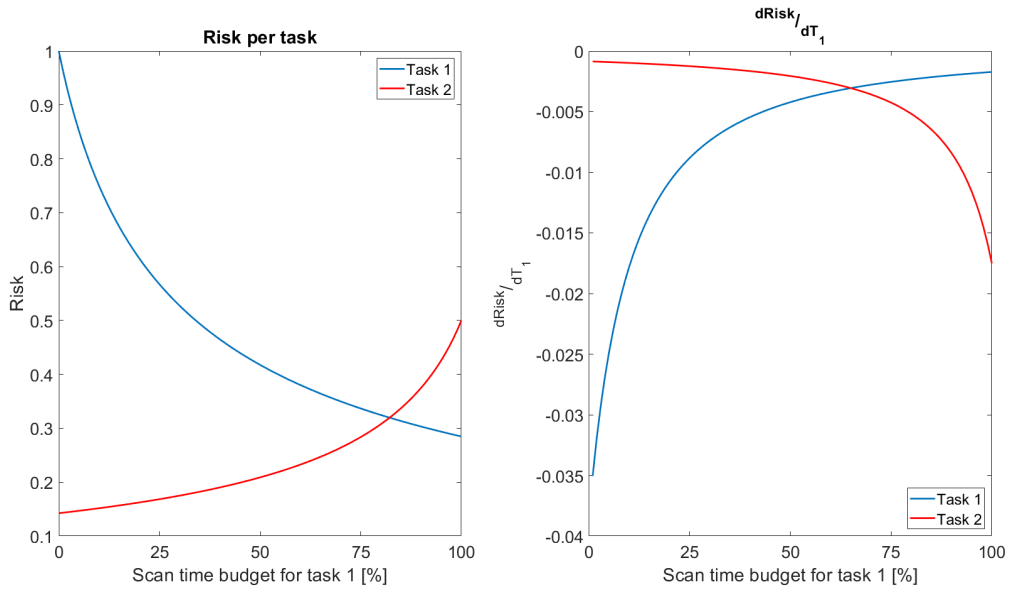

Figure 6.1: Risk individual tasks: Scenario 1A

Figure 6.2 illustrates the same figures for scenario 1B. The reduction in available scan time budget results in a flattening of the risk curves. The risk of task 1 is above the risk of task 2 within the entire domain of the scan time budget of T_1 in the figure on the left. The derivatives in the figure on the right for both tasks are equal at $T_1 = 0.963T$.

Figures 6.3a and 6.3b illustrate the cost functions used in equations 4.12 and 4.13 using the parameters of scenarios 1A and 1B.

The value of T_1 that results in a minimum for the *Sum* method in the figure on the left in Figure 6.3a is equal to the value of T_1 where the derivatives of both tasks are equal in the figure on the right in Figure 6.1.

The value of T_1 that results in a minimum for the *Max* method in the figure on the left in Figure 6.3a is equal to the value of T_1 where the risks of both tasks are the same in the figure on the left in Figure 6.1.

Similarly for scenario 1B, the value of T_1 that results in a minimum for the *Sum* method in the figure on the right in Figure 6.3b is equal to the value of T_1 where the derivatives in the figure on the right in Figure 6.2 are equal.

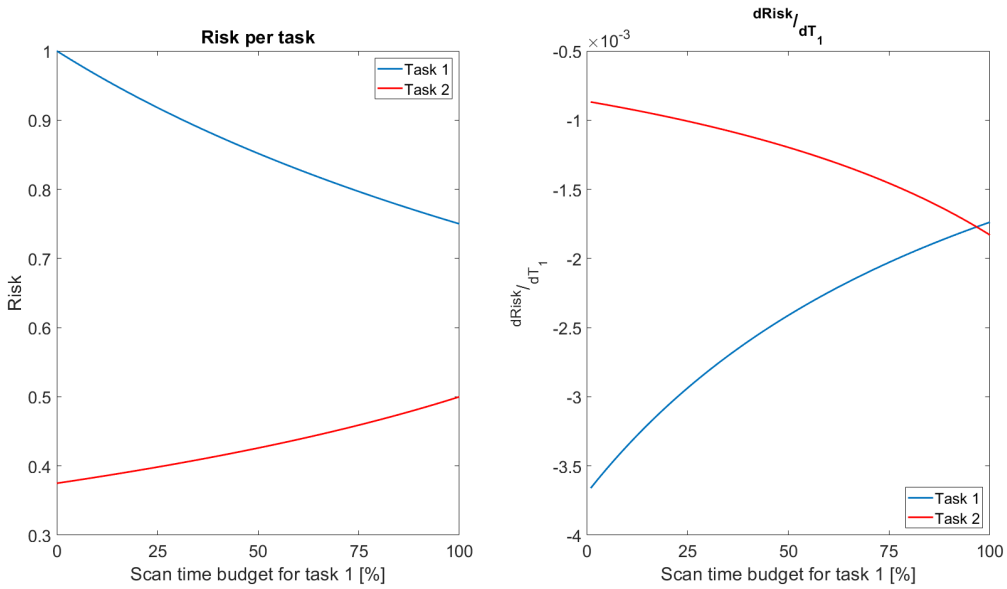

Figure 6.2: Risk individual tasks: Scenario 1B

The absence of a risk crossing in the figure on the left in Figure 6.2 caused by the reduced available scan time budget results in $T_1 = T$ for the *Max* method.

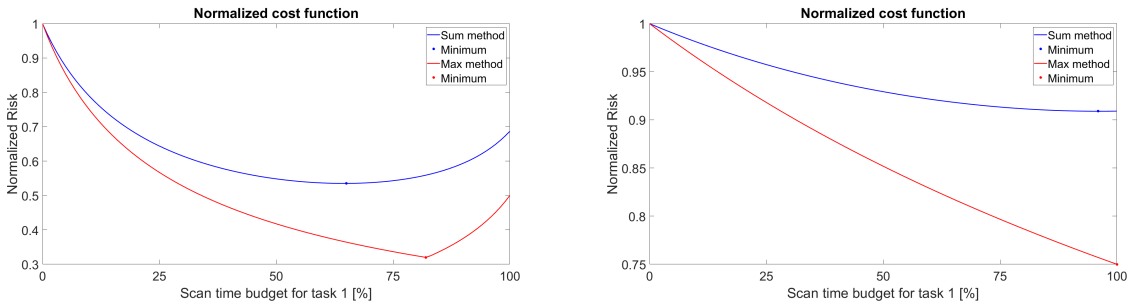

(a) Scenario 1A

(b) Scenario 1B

Figure 6.3: Normalized cost functions for scenarios 1A and 1B

Both the *Sum* and *Max* method in scenarios 1A and 1B allocated more than 50% of the scan time budget to task 1, caused by the higher costs of missed detection and false alarms in Table 6.4 compared to Table 6.5.

The costs achieved after the measurement for both scenarios are illustrated in figure 6.4. The *Sum*, *Max* and *Uniform* bins refer to the method of allocating the scan time budget. The *Sum* method allocates the budget to minimize the *sum of tasks cost* and the *Max* method allocates the budget to minimize the *maximum task cost*.

The *Sum* method in both figures on the left in Figures 6.4a and 6.4b achieves the lowest *sum of tasks cost*. The *Max* method in both figures on the right in Figures 6.4a and 6.4b achieves the lowest *maximum task cost*.

Figure 6.4 illustrates that the *Sum* method only minimizes the expected total cost and that the *Max* method only minimizes the maximum cost of all individual tasks, highlighting the precision of each method to minimize only its assigned cost criteria.

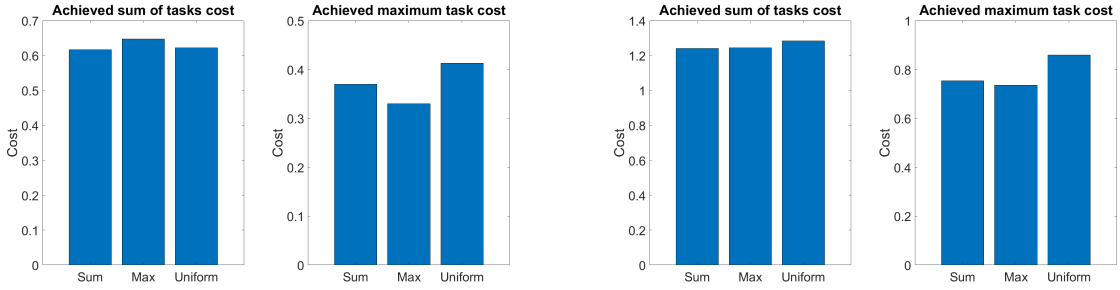

(a) Scenario 1A

(b) Scenario 1B

Figure 6.4: Achieved cost for scenarios 1A and 1B

6.2 Multiple decisions per task

This section simulates a scenario with two tasks with each 991 range cells, for a single scan, as shown in Table 6.6. The *Sum* and *Max* methods distribute the scan time budget solving Equations 5.3 and 5.4.

Tasks	Range cells per task	Scans	Birth/Death	Optimization *Sum*	Optimization *Max*
2	991	1	×	Eq 5.3	Eq 5.4

Table 6.6: Simulation parameters scenario 2

Task	$P(H_{1,x})$	$C_{miss,x}$	$C_{fa,x}$	$SNR(T, 0.75R_{max})$	$P_{birth,x}$	$P_{death,x}$
1	Fig 6.5, $x < 0$	Fig 6.5, $x < 0$	Fig 6.5, $x < 0$	1	0	0
2	Fig 6.5, $x > 0$	Fig 6.5, $x > 0$	Fig 6.5, $x > 0$	10	0	0

Table 6.7: Object parameters scenario 2

The object parameters for scenario 2 are presented in Table 6.7. The prior probability of object presence, cost of a missed detection and cost of a false alarm as function of position are illustrated in figure 6.5. Task 1 is associated with the object presence decisions for $x < 0$ and task 2 for $x > 0$.

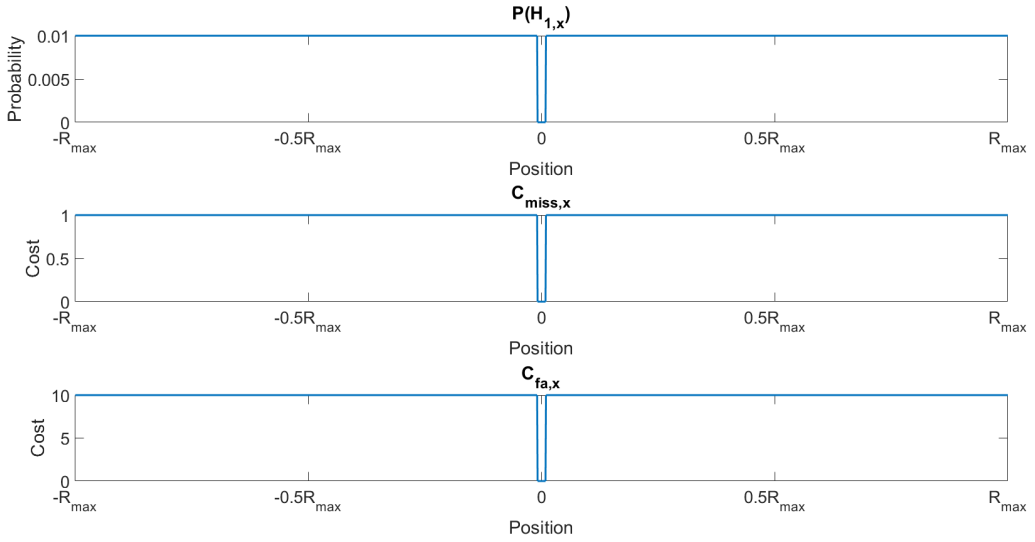

Figure 6.5: Parameters for scenario 2

The difference between the object parameters for scenario 2 for both tasks is the difference in RCS. For task 1, $SNR_1(T_1 = T, R = 0.75R_{max}) = 10$ and $SNR_1(T_1 = T, R = 0.75R_{max}) = 1$, with R_{max} the maximum range.

Figure 6.6 illustrates the risk in cells within a single task as a function of the allocated scan time budget. The top figure illustrates the risk at multiple cells in scan direction 1 as a function of the scan time budget allocated to task 1, and the bottom figure illustrates the risk at multiple cells in scan direction 2.

As the scan time budget allocated to task 1 increases, the risk curve of each cell in the top figure decreases. The blue curve illustrates the risk curve for the cell with the shortest range. A scan time budget of $T_1 = 0.001T$ reduces the risk of this cell to $5.77 \times 10^{-}6$, locally resulting in a large negative slope. The red curve illustrates the risk of the cell in a range of $R = 0.25R_{max}$. The increased range compared to the blue curve results in a higher risk. With a full scan time budget of $T_1 = T$, there is a remaining risk of 0.0014 for the red curve, reflecting that there is not enough budget to reduce the risk of the red curve asymptotically to zero within a single scan. The green curve illustrates the risk

of the cell at $R = R_{max}$, which has approximately a horizontal risk curve, reflecting the inability of the amount of the scan time budget available to reduce the risk for cells at long range.

The lower figure in Figure 6.6 illustrates the risk curves in scan direction 2 as a function of T_1, using $T = T_1 + T_2$. Increased SNR for a potential object in scan direction 2 results in a lower risk for a cell in scan direction 2 compared to a cell in scan direction 1, under the assumption that both cells have the same range and scan time budget available. For example, the curves in the lower figure at $T_1 = 0.75T$ have a lower risk compared to the curves in the upper figure with matching color at $T_1 = 0.25T$.

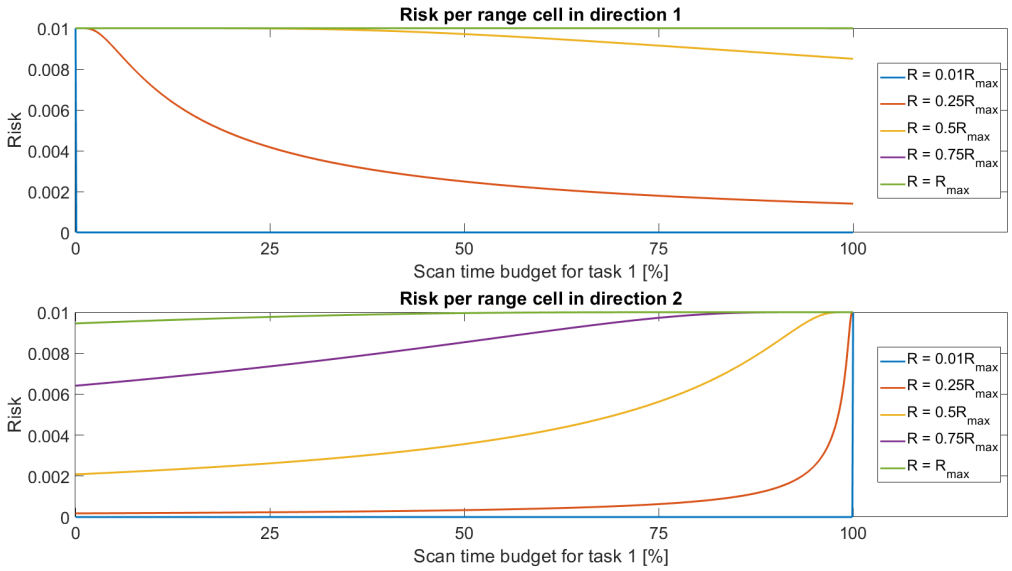

Figure 6.6: $Risk(T_1)$ for multiple range cells

Figure 6.7 illustrates the risk as a function of the position for various values of T_1. The area under each curve for $x < 0$ is equal to the expected risk for task 1 defined by equation 5.2. The area under each curve for $x > 0$ is equal to the expected risk for Task 2.

The purple curve in Figure 6.7 illustrates the risk when the entire scan time budget is allocated to task 1. The risk for cells at close range for $x < 0$ are reduced to approximately zero, due to the high SNR obtained. The risk remains approximately 0.01 in cells with $R \geq 0.6R_{max}$, due to the low SNR obtained. In between, there is a transition between a relatively low risk of approximately zero and a relatively high risk of approximately 0.01. The reduction of T_1 to $T_1' > 0$ results in a horizontal compressed risk curve for $x \in [-R_{max}, 0.01R_{max}]$. The reduction of T_1 results in the increase of T_2, resulting in a horizontal expansion of the risk curves for task 2 with $x \in [0.01R_{max}, R_{max}]$. The *Sum* and *Max* methods each make a different trade-off decision for the horizontal expansion and retraction of the risk curves for both tasks.

The figure on the right in Figure 6.8 illustrates the expected risk, $t_1'^{BR}(T_1)$ and $t_2'^{BR}(T - T_1)$, as defined in equation 5.2. Task 1 has a large decrease in risk near $T_1 = 0$ caused by the reduction in the risk of cells at close range. $t_1'^{BR}(0.001) - t_1'^{BR}(0)$ equals the area between the blue and red curves for $x < 0.01R_{max}$ in the figure on the right in Figure 6.7. For task 2 a similar reasoning holds for the large increase in risk near $T_1 = 1$.

The figure on the left in Figure 6.8 illustrates the normalized *Sum* and *Max* cost functions. The *Sum* cost function is obtained by taking the sum of both tasks in the figure on the right in Figure 6.8. The *Max* cost function is obtained by taking the maximum of both tasks in the figure on the right in Figure 6.8. The *Sum* method has a minimum at $T_1 = 0.36T$. The *Max* method has a minimum at $T_1 = 0.91T$.

This scenario demonstrates that the *Sum* and *Max* methods allocate more of the scan time budget to different tasks. The lower RCS for cells in scan direction 1 resulted in a lower scan time budget allocated by the *Sum* method. The lower RCS for cells in scan direction 1 resulted in a higher scan time budget allocated by the *Max* method.

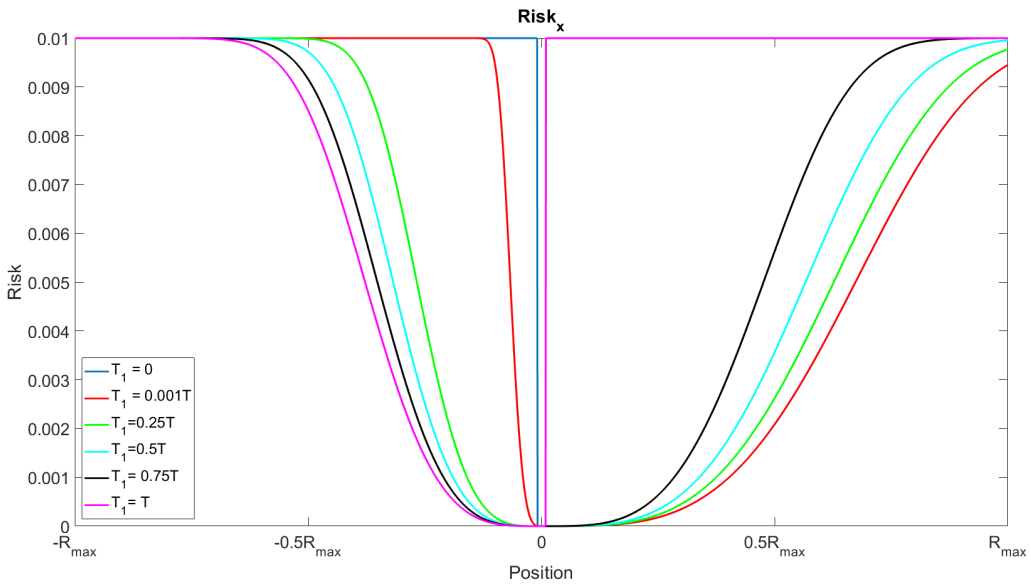

Figure 6.7: $Risk_x$ for multiple T_1 choices

The resulting risk curves as a function of the position for the chosen values of T_1 are illustrated in Figure 6.9. By allocating T_1 by solving equation 5.4, the *Max* method achieved a risk curve in Figure 6.9 that has equal risk for both tasks. The equal risk per task is visualized by equal areas under the red curve for $x < -0.01R_{max}$ and $x > 0.01R_{max}$.

By allocating T_1 by solving equation 5.3, the *Sum* method achieved a risk curve in Figure 6.9 that has the minimum combined expected risk for tasks 1 and 2. The *Sum* method allocates less budget to task 1, resulting in an increase in the expected risk for task 1. The increase in expected risk for task 1 is equal to the area between the blue and red curves for $x < -0.01R_{max}$ in Figure 6.9. The area between the red and blue curves for $x > 0.01R_{max}$ is larger than the area for $x < -0.01R_{max}$, resulting in a lower combined expected risk for the *Sum* method.

Figure 6.10 illustrates the cost achieved after the scan, using the value of T_1 corresponding to the *Sum*, *Max* and *Uniform* methods. The figure on the left illustrates the total cost achieved. The figure on the right illustrates the maximum cost of either task.

The figure on the left in Figure 6.10 illustrates that the choice of T_1 made by the *Sum* method results in the lowest achieved *sum of tasks cost*. The figure on the right in Figure 6.10 illustrates that the choice of T_1 made by the *Max* method results in the lowest achieved *maximum task cost*.

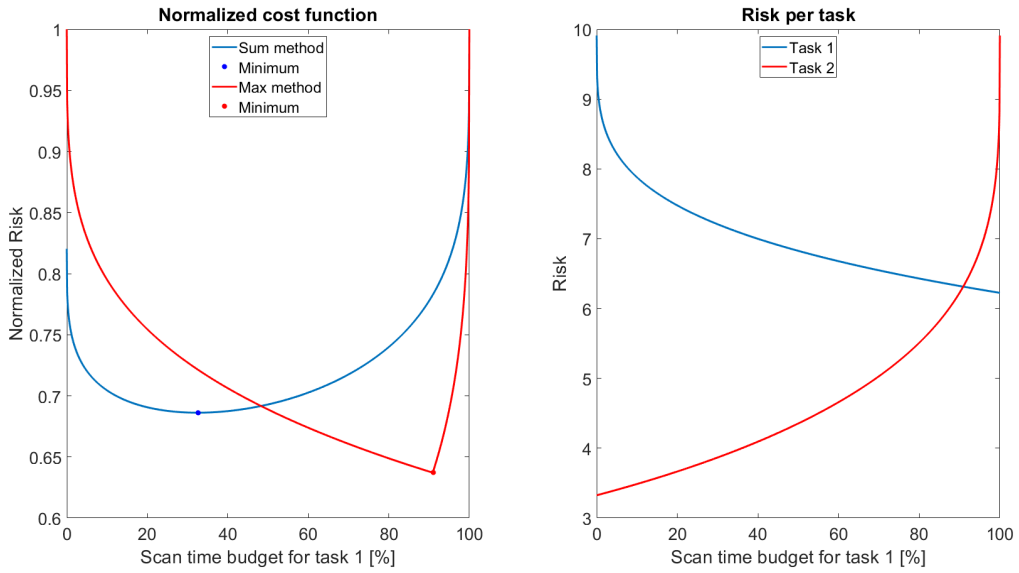

Figure 6.8: Risk at system and task level

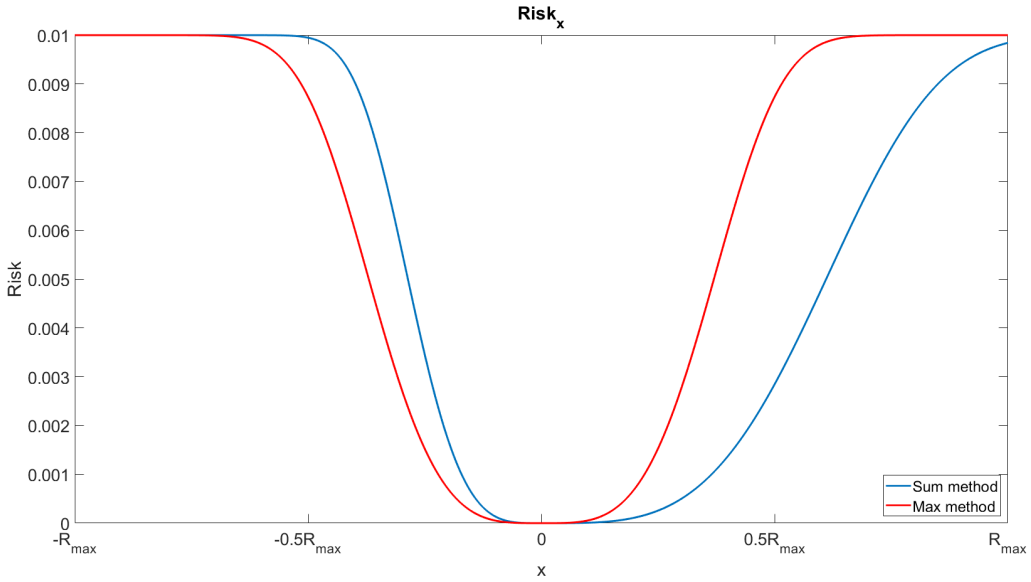

Figure 6.9: Risk with chosen T_1

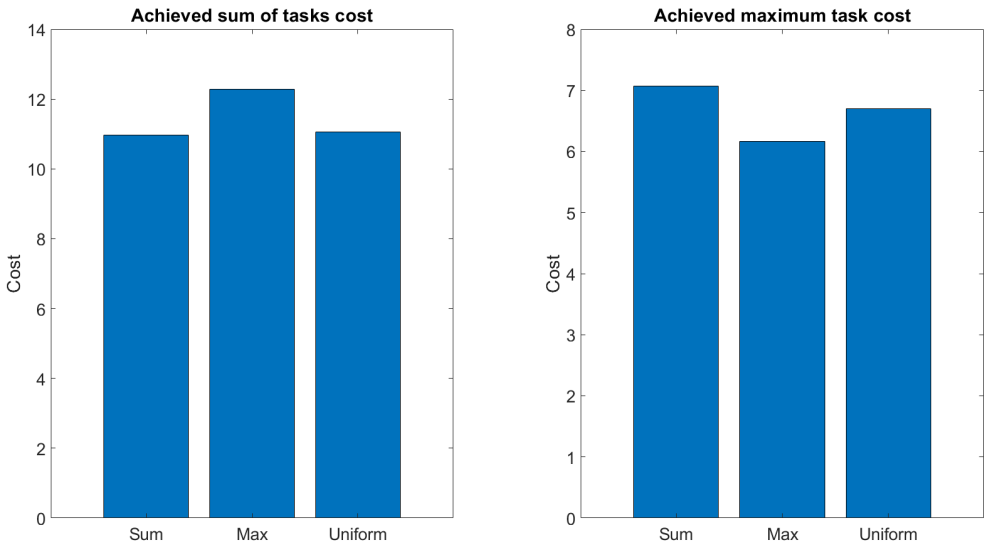

Figure 6.10: Achieved cost

6.3 Sequential scans and birth-death process

This Section simulates two scenarios, each with two tasks with 991 range cells per task, for 32 and 48 scans. Subsection 6.3.1 considers scenario 3A, with simulation parameters shown in Table 6.8. Subsection 6.3.2 considers scenario 3B, with simulation parameters shown in Table 6.9. The main difference between scenarios 3A and 3B is the nonzero probability of object birth and death for scenario 3B.

Tasks	Range cells per task	Scans	Birth/Death	Optimization *Sum*	Optimization *Max*
2	991	32	×	Eq 5.8	Eq 5.9

Table 6.8: Simulation parameters scenario 3A

Tasks	Range cells per task	Scans	Birth/Death	Optimization *Sum*	Optimization *Max*
2	991	64	✓	Eq 5.17	Eq 5.18

Table 6.9: Simulation parameters scenario 3B

6.3.1 Sequential measurements

The object parameters for this scenario are shown in Table 6.10. The object parameters for both tasks are equal, except for the cost coefficients $C_{miss(x)}$ and $C_{fa,x}$ and the prior probability $P(H_{1,x})$, as illustrated in Figure 6.11. Task 1 has a range interval of $x \in [-0.505R_{max}, -0.01R_{max}]$. Task 2 has a range interval of $x \in [0.505R_{max}, R_{max}]$.

Task	$P(H_{1,x})$	$C_{miss,x}$	$C_{fa,x}$	$SNR(T, 0.5R_{max})$	$P_{birth,x}$	$P_{death,x}$
1	Fig 6.11 , $x < 0$	Fig 6.11, $x < 0$	Fig 6.11, $x < 0$	10	0	0
2	Fig 6.11, $x > 0$	Fig 6.11, $x > 0$	Fig 6.11, $x > 0$	10	0	0

Table 6.10: Object parameters scenario 3A

Figure 6.12 illustrates the risk and object probability map before the first, second and third scan, using the *Uniform* method for scan time budget allocation.

Given that an object is present in a cell results in that the probability that an object is present converges to 1 as the number of scans increases. Given that an object is absent in a cell results in that the probability that an object is present converges to 0 as the number of scans increases. The probability that an object is present in cells with smaller range will converge with fewer scans. This is illustrated in the bottom center figure in Figure 6.12. The object probability map for cells in the interval $x \in [-0.01R_{max}, -0.2R_{max}]$ is approximately 0 or 1, resulting in 0 risk in deciding the presence or absence of an object. For cells with a larger range, more scans are required for $P(H_{1,x})$ to converge to 0 or 1. The risk of each individual task for a static scenario converges to zero as the number of scans goes to infinity.

Figure 6.13 illustrates the normalized cost functions for the first six scans for an individual simulation run. Both tasks contain the same risk before the first scan. The *Max* method has a minimum at $T_1 = 0.01T$ for the first scan. The probability of an object being present for cells in scan direction 1 at short range converge to either 0 or 1, resulting in zero risk in cells at close range for subsequent scans. The probability of an object being present for cells in scan direction 2 requires more scans to converge to either 0 or 1, resulting in a higher risk in the second, third, fourth and fifth scan. The difference in risk between both tasks is small enough in the sixth scan that $T_1 = 0.02T$, meaning that both tasks receive scan time.

The *Sum* method in Figure 6.13 has a minimum at $T_1 = T$ for the first two scans. As task 1 consists of cells with shorter range compared to cells of task 2, the *Sum* method first reduces the risk in task 1. After two scans, the *Sum* method switches to $T_1 = T$, reducing the risk for task 2, which requires more scan time to reduce the same amount of risk compared to task 1.

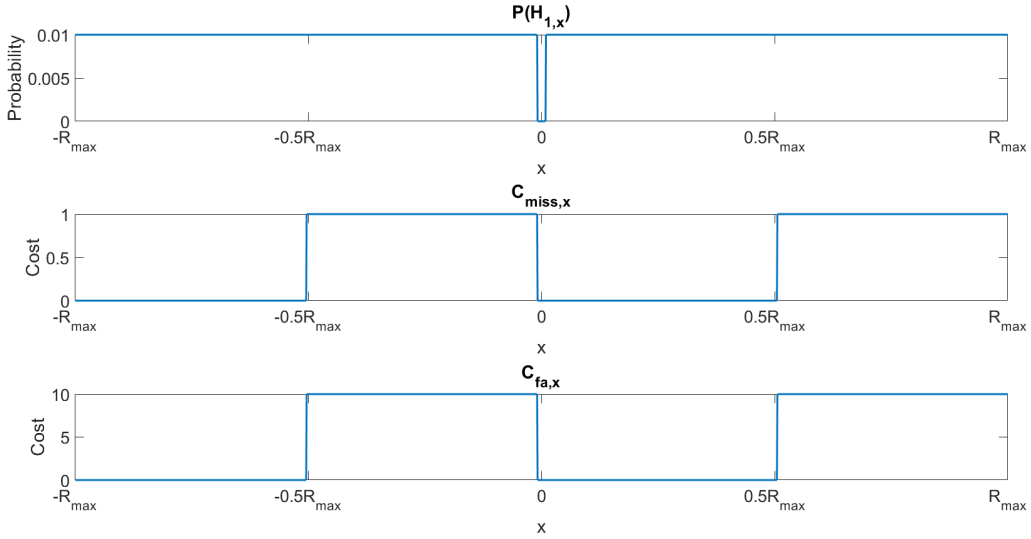

Figure 6.11: Parameters for scenario 3A and 3B

Figure 6.14 illustrates that on average the *Sum* method allocates 100%, 77% and 23% of the budget to task 1 in the first three scans to reduce the risk of cells in close range. An average of $T_1 = 0.13T$ is obtained for the *Sum* method for the subsequent scans. The *Max* method on average allocates less than 5% to task 1 for all 32 scans. The cells in task 2 are at a longer range compared to the cells in task 1, requiring more scan time budget to even the risk in both tasks.

Figure 6.15 illustrates the allocation of T_1 of individual simulation runs for the *Sum* method in the figure on the left and for the *Max* method in the figure on the right. The color illustrates the percentage of T allocated to T_1.

The image in the figure on the left in Figure 6.15 illustrates that using the *Sum* method to find T_1 often results in assigning most of T to a single task, visualized by the dominant dark blue, orange, and yellow colors. This image illustrates that the T_1 values for the *Sum* method for single simulation runs are not equal to the average values in Figure 6.14.

The image in the figure on the right in Figure 6.15 illustrates that using the *Max* method to find T_1 for individual simulation runs deviates less from the average value in Figure 6.14 for the first 18 scans, compared to the *Sum* method. After 18 scans, individual simulation runs with outliers of $T_1 > 0.5T$ become more frequent.

Figure 6.16 illustrates the achieved *sum of tasks cost* in the figure on the left, and the achieved *maximum task cost* in the figure on the right. The *Sum* method has the lowest achieved *sum of tasks cost* for each individual scan. The *Max* method achieves a lower achieved *sum of tasks cost* compared to the *Uniform* method after the 19^{th} scan, caused by the constant 50% allocation of T to task 1 by the *Uniform* method. The *Max* method in the figure on the right of Figure 6.16 has the lowest achieved *maximum task cost* for each scan.

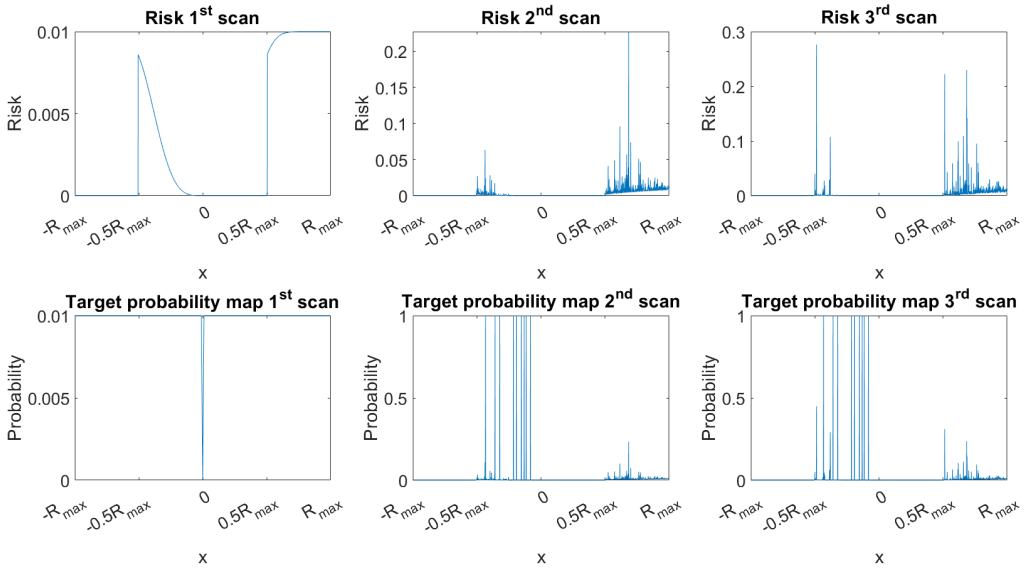

Figure 6.12: $Risk_x$ and object probability map

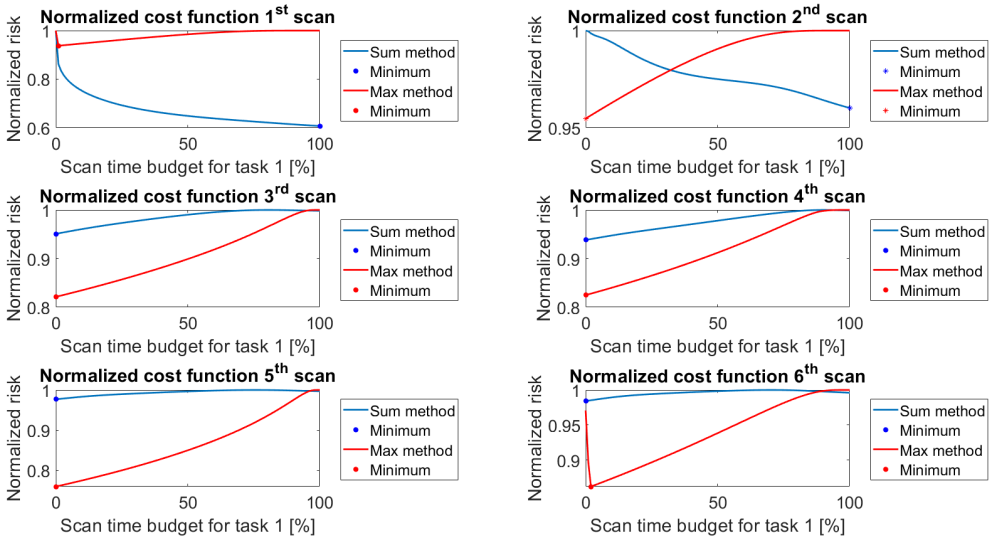

Figure 6.13: Normalized cost function: Scenario 3A

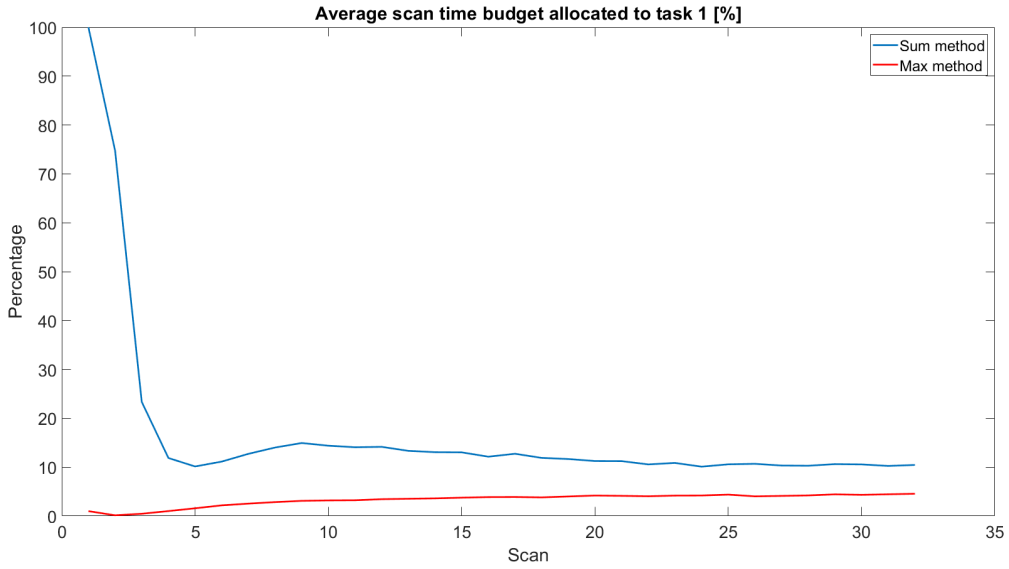

Figure 6.14: Average scan time budget allocation: Scenario 3A

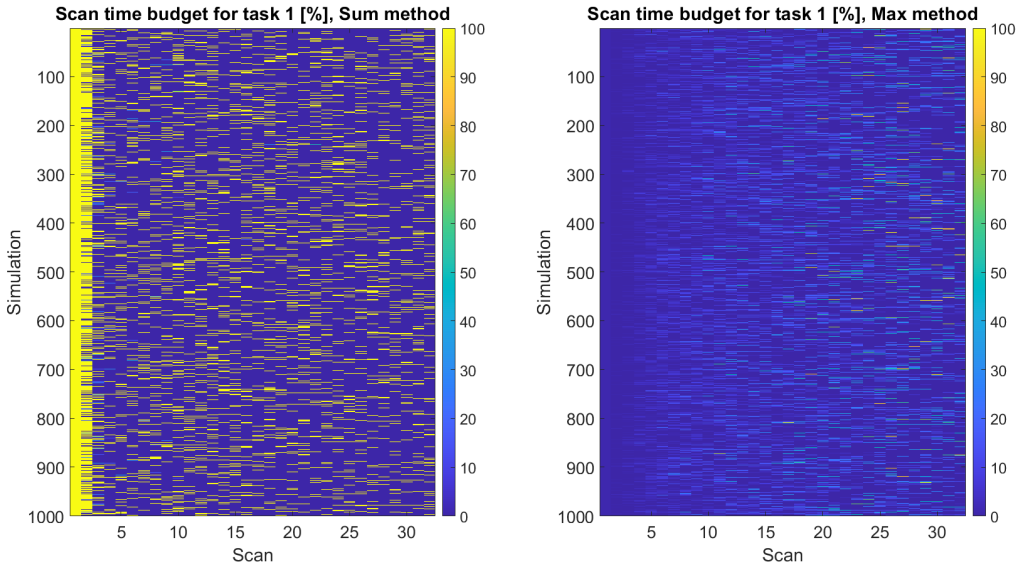

Figure 6.15: Scan time budget allocation for individual simulations: Scenario 3A

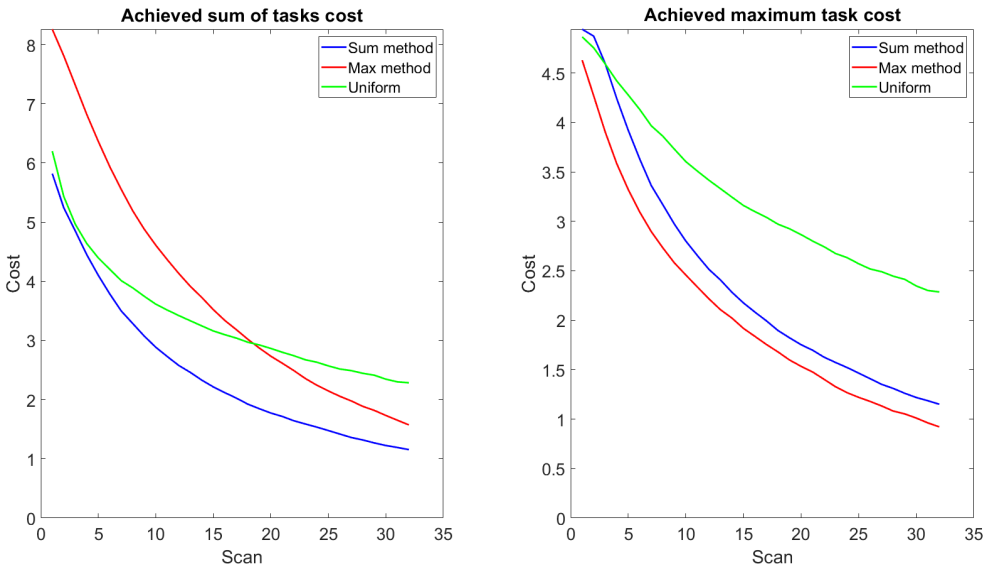

Figure 6.16: Achieved cost: Scenario 3A

6.3.2 Object birth-death process

The object parameters for this scenario are shown in Table 6.11. The object parameters in Table 6.11 are equal to the object parameters of scenario 3A in Table 6.10, except $P_{birth,x}$ and $P_{death,x}$.

Task	$P(H_{1,x})$	$C_{miss,x}$	$C_{fa,x}$	$SNR(T, 0.5R_{max})$	$P_{birth,x}$	$P_{death,x}$
1	Fig 6.11, $x < 0$	Fig 6.11, $x < 0$	Fig 6.11, $x < 0$	10	Fig 6.17, $x < 0$	Fig 6.17, $x < 0$
2	Fig 6.11, $x > 0$	Fig 6.11, $x > 0$	Fig 6.11, $x > 0$	10	Fig 6.17, $x > 0$	Fig 6.17, $x > 0$

Table 6.11: Object parameters scenario 3B

$P_{birth,x}$ and $P_{death,x}$ for scenario 3B are illustrated in figure 6.17. Both tasks have an equal probability of object birth and death as a function of the range. $\frac{P_{death,x}}{P_{birth,x}} = 0.99$ in the position intervals $x \in [-R_{max}, -0.01R_{max}]$ and $[0.01R_{max}, R_{max}]$ resulting in the same prior probability of an object being present in each cell as the top figure in Figure 6.11.

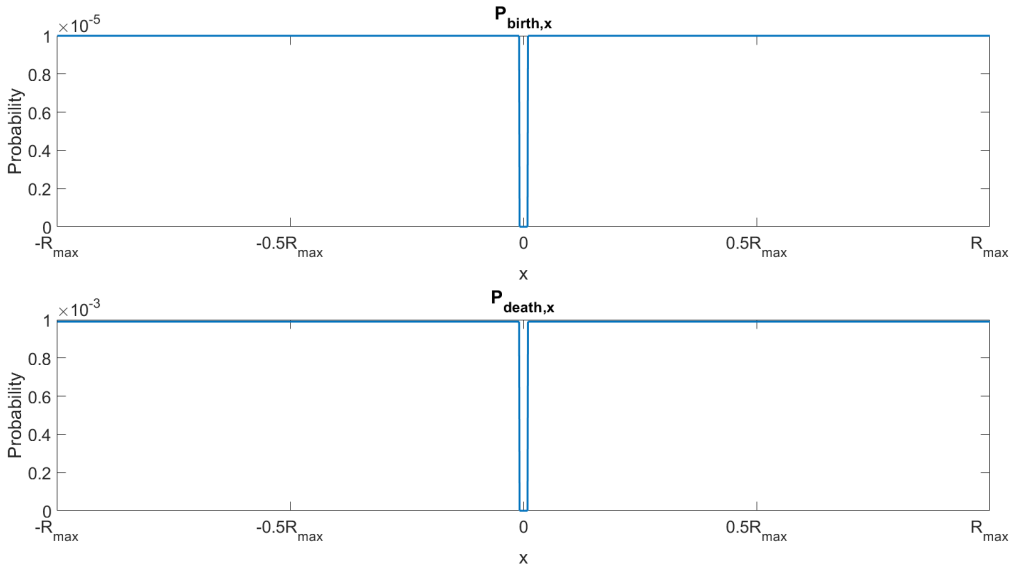

Figure 6.17: Object birth and object death probabilities

In scenario 3A, when the probability of the presence of an object in a cell is 0 or 1, it stays constant for subsequent scans. For scenario 3B, the probability of the presence of an object does not remain 0 or 1, which is illustrated in Figure 6.18. The figures on the left illustrate the risk and object probability map after the 31^{st} scan. The figures on the right illustrate the risk and object probability map before the 32^{nd} scan.

Given that the probability of the presence of an object is 1 after the 31^{st} scan, the birth-death process causes the probability to decrease to $(1 - P_{death,x})$ before the 32^{nd} scan. Given that the probability of the presence of an object is 0 after the 31^{st} scan, the birth-death process causes the probability to increase to $P_{birth,x}$ before the 32^{nd} scan.

The chosen $P_{death,x}$, $P_{birth,x}$ illustrated in Figure 6.17, combined with $C_{fa,x}$ and $C_{miss,x}$, result in a greater increase in risk for the cells with a probability of the presence of an object close to 1 compared to cells with a probability close to 0.

Figure 6.19 illustrates the normalized cost functions for the 1^{st}, 2^{nd}, 3^{rd}, 30^{th}, 31^{st} and 32^{nd} scans for an individual simulation run. The difference between the normalized cost functions for scenarios 3A and 3B in Figures 6.13 and 6.19 increases with the number of scans. The normalized cost functions in Figure 6.13 approach 1 for the 30^{th}, 31^{st} and 32^{nd} scan. The normalized cost functions in Figure 6.19 have a larger range for the y-axis, indicating a greater potential risk reduction for the 30^{th}, 31^{st} and 32^{nd} scan in scenario 3B compared to scenario 3A. In scenario 3A, the remaining risk for the 30^{th},

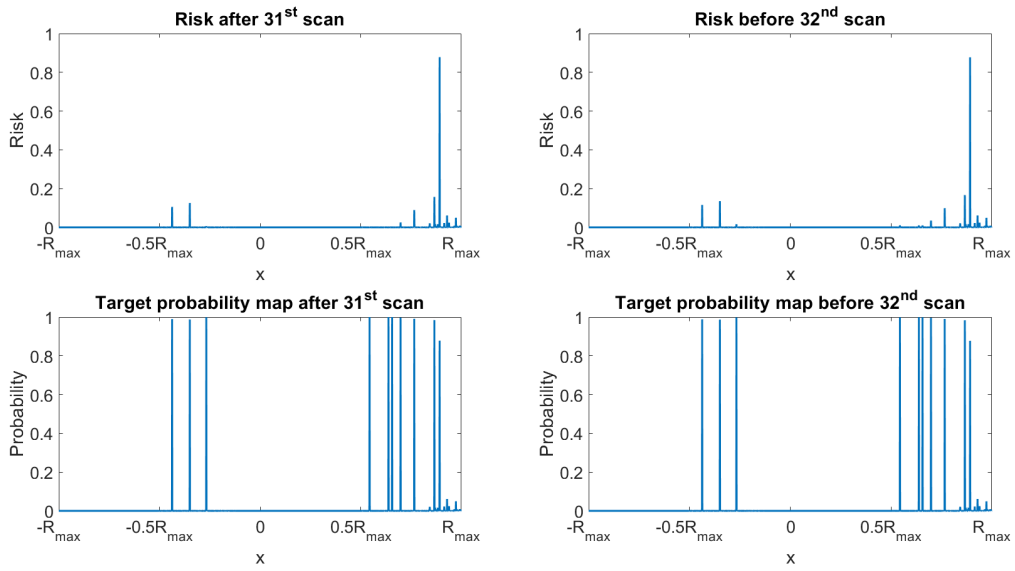

Figure 6.18: $Risk_x$ and object probability map

31^{st} and 32^{nd} is in cells with a larger range. On the contrary, the birth-death process in scenario 3B introduces risk at cells both at short and high range after each scan, resulting in nonzero risk in cells at short range. The nonzero risk for cells in short range results in a larger expected risk reduction within a single scan compared to scenario 3A.

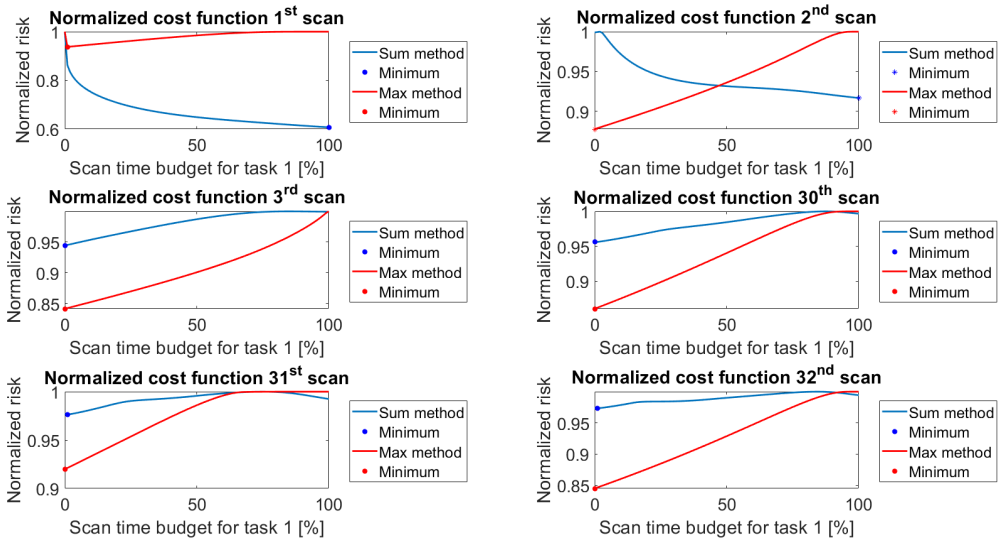

Figure 6.19: Normalized cost function: Scenario 3B

Figure 6.20 illustrates the allocation of the scan time budget averaged over 10000 simulation runs. The allocation of T_1 using the *Max* method in Figure 6.20 is not significantly changed by the introduction of nonzero values for $P_{birth,x}$ and $P_{death,x}$ in this scenario. The allocation of T_1 using the *Sum* method in Figure 6.20 does not average at $t_1 = 0.13T$ as in Figure 6.14, but increases to $T_1 = 0.665T$. The *Sum* method increases T_1 to $0.665T$ to reduce the risk of task 1, induced by the birth-death process for cells in scan direction 1, which have a smaller range compared to cells in scan direction 2.

Figure 6.21 illustrates the allocation of the scan time budget for individual simulations for scenario 3B. The allocation using the *Sum* method is illustrated on the left, the allocation using the *Max* method is illustrated on the right. The dominant presence of dark blue and bright yellow in the figure on the

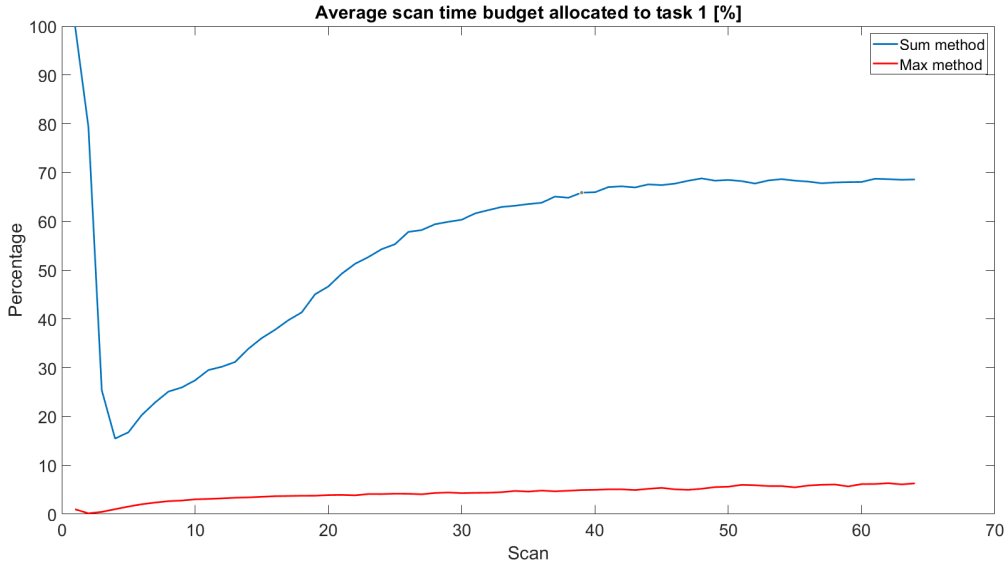

Figure 6.20: Average scan time budget allocation: Scenario 3B

left indicates the preference of the *Sum* method to allocate the entire budget to a single task. The scan time budget allocation using the *Max* method in Figure 6.21 is similar to the right figure in Figure 6.15 for the first 32 scans. Between the 32^{nd} and 64^{th} scan, the average scan time budget allocation in Figure 6.20 increases from 4.7% and 6.8%. The figure on the right illustrates that the *Max* method between the 32^{nd} and 64^{th} scan starts to allocate more than 50% of the scan time budget to task 1 more frequently.

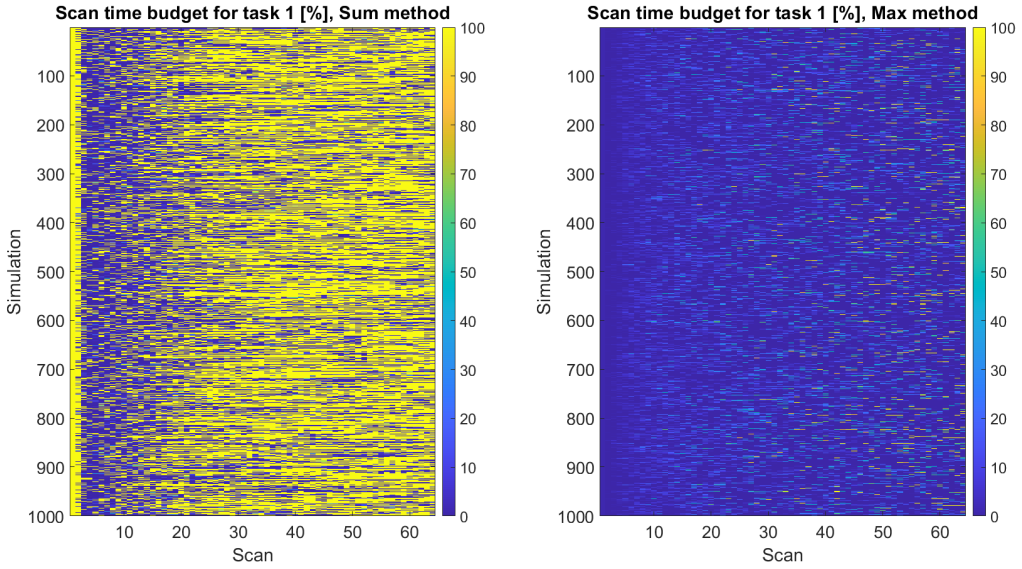

Figure 6.21: Scan time budget allocation for individual simulations: Scenario 3B

Figure 6.22 illustrates the achieved *sum of tasks cost* in the figure on the left and the achieved *maximum task cost* in the figure on the right. The *Max* method achieves a lower *sum of tasks cost* than the *Sum* method after 42 scans. The *Sum* method allocates on average 67.5% of the budget to task 1 after 42 scans, resulting in a higher achieved cost for task 2 compared to the *Max* method. The lower achieved *sum of tasks cost* after 42 scans for the *Max* method compared to the *Sum* method motivates to formulate a non-myopic cost function for both the *Sum* and *Max* method.

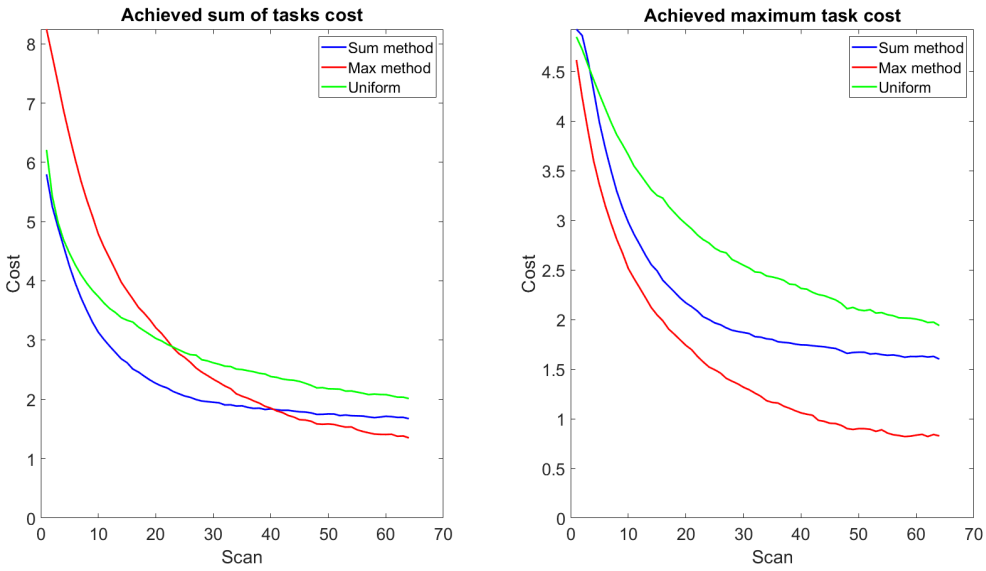

Figure 6.22: Achieved cost: Scenario 3B

6.4 Three tasks

The simulation parameters are shown in Table 6.12. This section simulates a scenario with three tasks, each with 991 range cells, for 48 scans. The first and third task include a birth-death process for individual cells. The scan time budget allocation is obtained by solving equations 5.17 and 5.18 for the *Sum* and *Max* method respectively.

Tasks	Range cells per task	Scans	Birth/Death	Optimization *Sum*	Optimization *Max*
3	991	48	✓	Eq 5.17	Eq 5.18

Table 6.12: Simulation parameters scenario 4

An overview of the object parameters is shown in Table 6.13. Cells within task 1 have an SNR ten times smaller compared to tasks 2 and 3 at equal range using the same scan time budget. Figure 6.23 illustrates that task 2 has twice the costs of $C_{miss,\{2,x\}}$ and $C_{fa,\{2,x\}}$ for individual cells compared to tasks 1 and 3. All cells have an equal prior probability of an object present of 0.01.

Task	$P(H_{1,x})$	$C_{miss,x}$	$C_{fa,x}$	$SNR(T, 0.5R_{max})$	$P_{birth,x}$	$P_{death,x}$
1	Fig 6.23	Fig 6.23	Fig 6.23	1	Fig 6.24	Fig 6.24
2	Fig 6.23	Fig 6.23	Fig 6.23	10	Fig 6.24	Fig 6.24
3	Fig 6.23	Fig 6.23	Fig 6.23	10	Fig 6.24	Fig 6.24

Table 6.13: Object parameters scenario 4

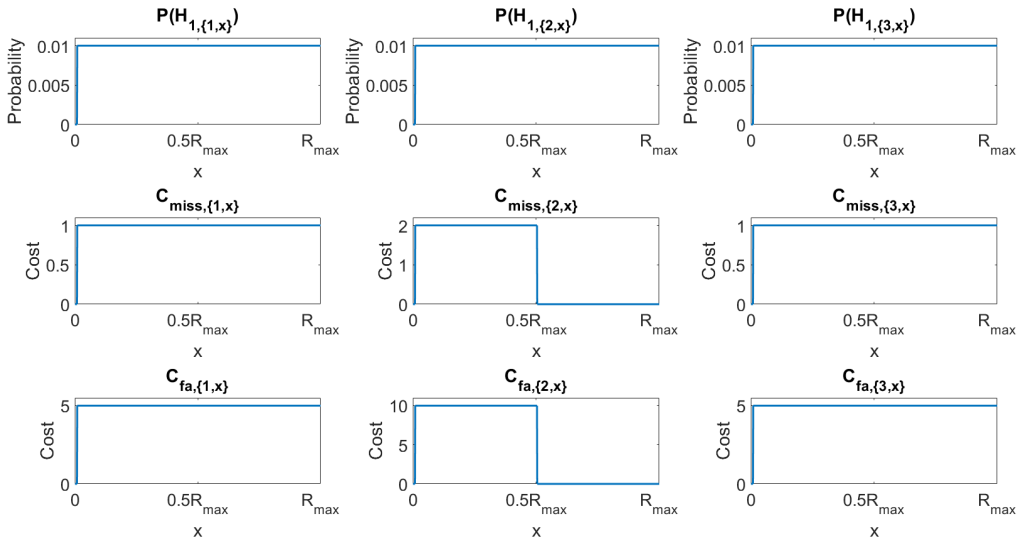

Figure 6.23: Object probability map and cost coefficients

Figure 6.24 illustrates the probability of object birth and death for the three tasks. The presence of objects for task 2 are constant over time, represented by $P_{birth\{2,x\}} = P_{death\{2,x\}} = 0$. The probability of object birth for individual cells within tasks 1 and 3 are $P_{birth\{1,x\}} = 1 \times 10^{-4}$ and $P_{birth\{3,x\}} = 2 \times 10^{-4}$. The probability of object death for individual cells within tasks 1 and 3 are $P_{death\{1,x\}} = 99P_{birth\{1,x\}}$ and $P_{death\{3,x\}} = 99P_{birth\{3,x\}}$. $P_{birth\{1,x\}}$ and $P_{birth\{3,x\}}$ are 10 and 20 times larger compared to scenario 3B, to emphasize the effect of a birth-death process on the scan time budget allocation.

Figure 6.25 illustrates the cost functions for the *Sum* and *Max* method for an individual simulation run, for the 1^{st} and 48^{th} scan. With three tasks, it holds that $T = T_1 + T_2 + T_3$, resulting in two optimization parameters. The horizontal axis in each figure in Figure 6.25 represents the percentage of T given to task 1, the vertical axis represents the percentage of T given to task 2. The remaining scan time budget is given to task 3. The color represents the risk associated to each method.

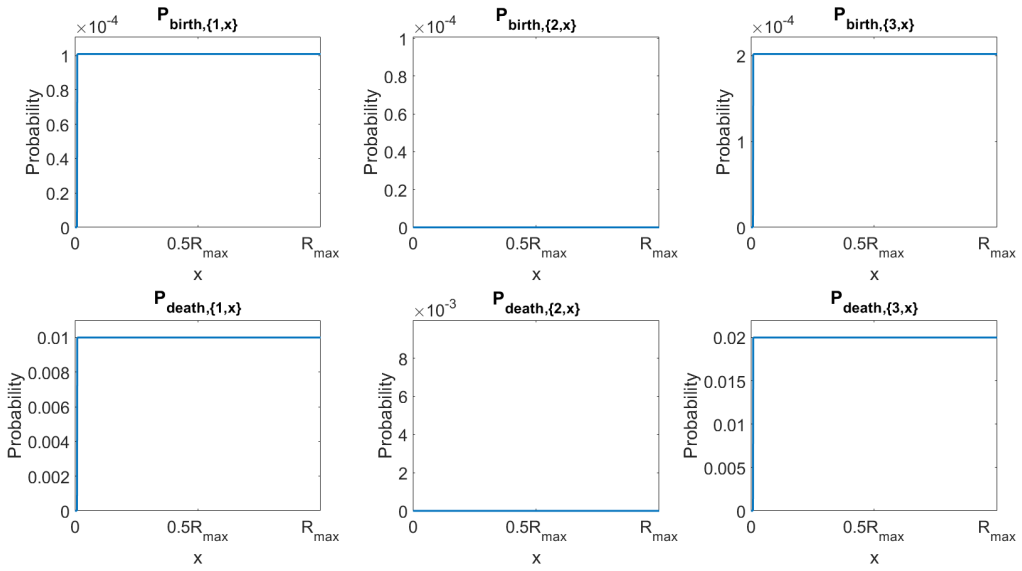

Figure 6.24: Object birth and object death probabilities

The top figure on the left in Figure 6.25 has local maxima if all scan time budget is allocated to a single task, which occurs at the corners of the triangle domain. The upper figure on the right in Figure 6.25 has the highest risk at the edges of the triangle domain, which occurs when at least one of T_1, T_2 or T_3 equals zero. The figures at the bottom of Figure 6.25 illustrate that both the *Sum* and *Max* method have a high cost when $T_3 = 0$ due to the large probabilities of object birth and object death for cells in scan direction 3.

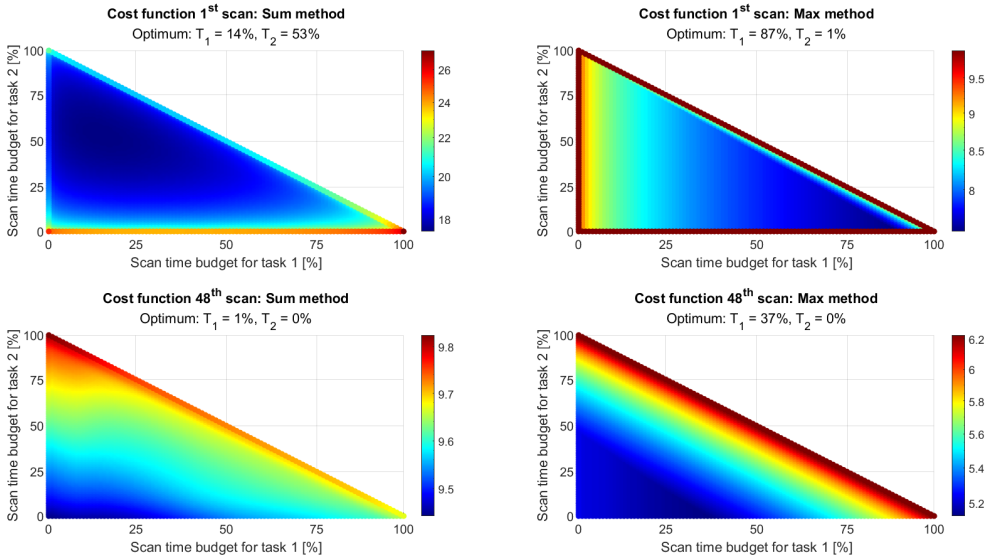

Figure 6.25: Normalized cost function 1^{st} and 48^{th} scan: Scenario 4

Figure 6.26 illustrates the average budget allocated using the *Sum* method for the figure on the left and using the *Max* method for the figure on the right. The *Sum* method in the figure on the left first prioritizes task 2, caused by the higher $C_{miss,\{2,x\}}$ and $C_{fa,\{2,x\}}$ for individual cells compared to tasks 1 and 3. As the number of scans increases, the average scan time budget allocated to task 2 for the *Sum* method decreases to 0.5% as cells in task 2 do not have a birth-death process. The lower RCS of individual cells and $P_{birth\{1,x\}}$ and $P_{death\{1,x\}}$ of individual cells in scan direction 1 compared to scan direction 3 results in a scan time budget allocation of 77% on average between the 32^{nd} and 48^{th} scan

for the *Sum* method.

The lower RCS for individual cells in scan direction 1 compared to individual cells in scan direction 3 results in a scan time budget allocation of 85% on average between the 32^{nd} and 48^{th} scan for the *Max* method in the figure on the right in Figure 6.26. The *Max* method allocates more scan time budget to task 3 as it requires more budget to reduce the risk as objects within scan direction 3 have a lower RCS compared to objects in scan direction 1.

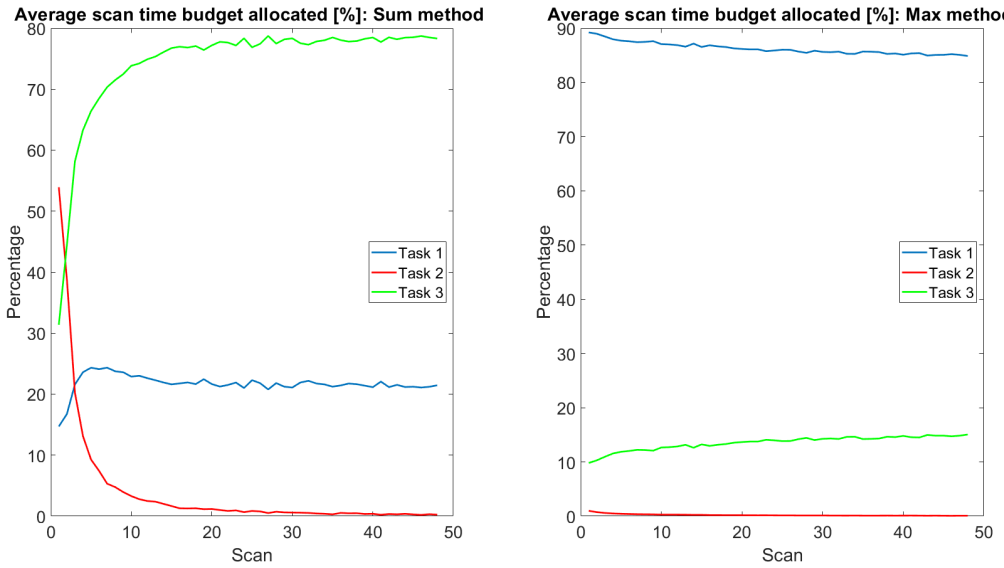

Figure 6.26: Average scan time budget allocation

Figure 6.27 illustrates the scan time budget allocation for individual simulation runs for the *Sum* method. Figure 6.28 illustrates the scan time budget allocation for individual simulation runs for the *Max* method. The *Sum* method allocates scan time to each task within the first three scans, rather than allocating the entire scan time budget to a single task as in the previous scenarios. The *Max* method has a maximum of 16% of scan time allocated to task 2, compared to 100% in scenario 3B.

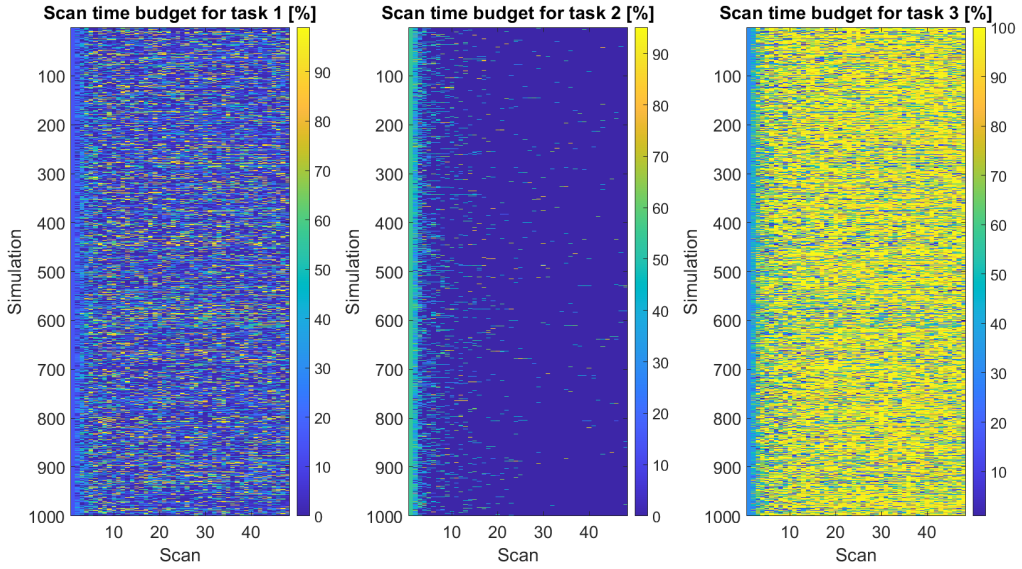

Figure 6.27: Scan time budget allocation for individual simulations using equation 5.17

Figure 6.29 illustrates the achieved *sum of tasks cost* in the figure on the left and the achieved *maximum task cost* in the figure on the right. Both figures illustrate that none of the *Sum*, *Max* and *Uniform*

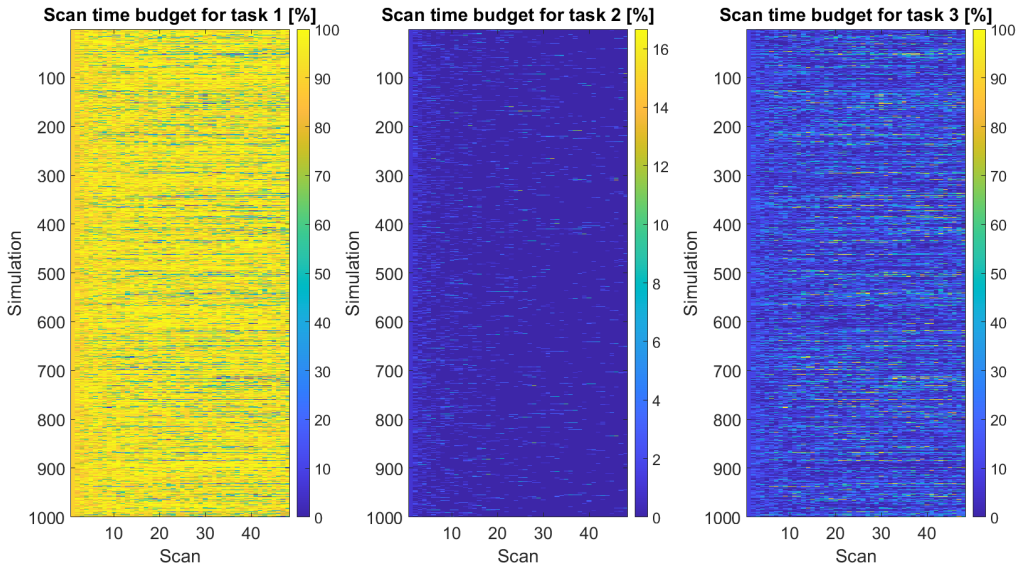

Figure 6.28: Scan time budget allocation for individual simulations using equation 5.18

methods converge to zero risk as the number of scans increases. The achieved *sum of task costs* at the 48^{th} scan are 10.3, 11.2 and 16.2 for the *Sum*, *Uniform* and *Max* methods respectively. The achieved *maximum task cost* at the 48^{th} scan are 5.7, 6.6 and 6.8 for the *Max*, *Uniform* and *Sum* methods respectively. The nonzero probabilities of object birth and object death causes the achieved costs in Figure 6.29 to not converge to zero.

Figure 6.29 illustrates that in this scenario, allocating the scan time budget using the *Sum* method results in the lowest achieved *sum of tasks cost* and allocating the scan time budget using the *Max* method results in the lowest achieved *maximum task cost*.

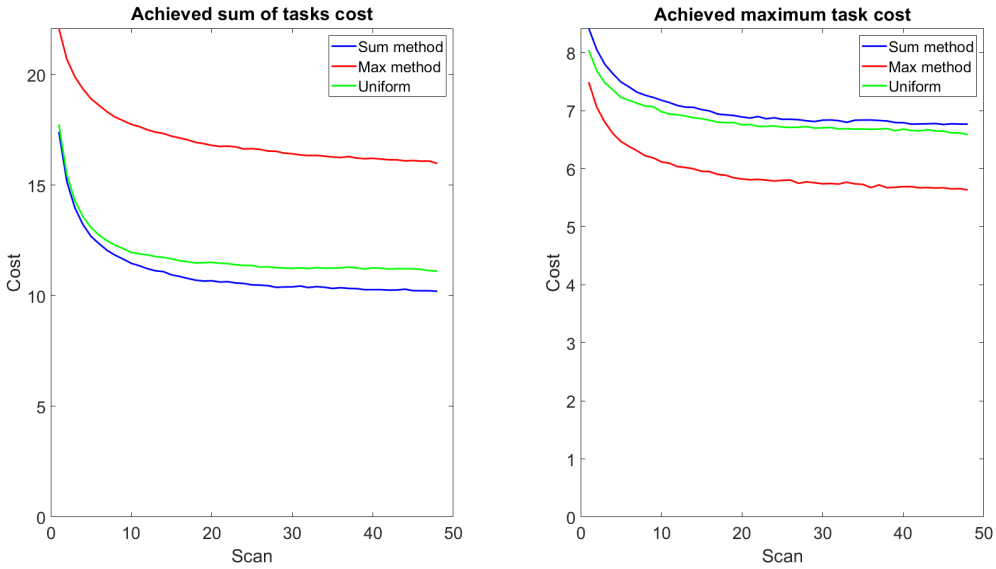

Figure 6.29: Achieved cost: Scenario 4

7 Conclusion and recommendations

This final chapter presents the conclusions and recommendations. Section 7.1 concludes the methodology and simulation results and reflects back on the research goal in the introduction. Section 7.2 gives recommendations for possible new generalizations of scenarios.

7.1 Conclusion

The expected performance of the individual object presence decision has been formulated as Bayes risk. Formulating for the first time, to our knowledge, the expected performance as Bayes risk enabled the cost function to include prior knowledge and previous measurements regarding the probability of an object being present. Furthermore, the expected performance of an individual decision formulated as Bayes risk enabled the radar user to prioritize individual decisions by assigning relative higher cost of a false alarm and missed detection. Both false alarms and missed detections have direct interpretations in the radar application, simplifying the assignment of costs to each event for radar users.

Using the definition of task performance as the sum of the Bayes risk of all object presence decisions within a single scan direction, two cost functions have been proposed at the system level. The *Sum* method takes the sum of the task performances. The *Max* method takes the maximum of the task performances. Chapter 5 has demonstrated that to extend the scenario with sequential scans and birth-death processes, the cost functions using the *Sum* and *Max* are obtained by reformulating the task performance. Given the reformulation of the task performances, the cost functions remain unchanged at the system level.

The *Sum* and *Max* method have demonstrated the flexibility to adapt the scan time allocation differently in simulations, depending on the scenario. For the first scan, the *Sum* method achieved a lower average *sum of tasks cost* compared to the *Max* and *Uniform* methods and the *Max* method achieved a lower average *maximum task cost* compared to the *Sum* and *Uniform* methods.

This research formulated myopic cost functions for the *Sum* and *Max* methods. The scenario in Subsection 6.3.2 demonstrated that a myopic implementation of the *Sum* method does not guarantee the lowest achieved *sum of tasks cost* for sequential scans. Similarly, a myopic implementation of the *Max* method does not guarantee the lowest achieved *maximum task cost* for sequential scans.

7.2 Recommendations

If this research work is continued, it is recommended:

- To implement a non-myopic cost-function. The simulations in this thesis only considered myopic cost functions. Predicting multiple scans ahead has lead to more sparse resource allocation and improved performance compared to the non-myopic cost function [2]. In a scenario as in Subsection 6.3.2, the *Sum* method, that allocates the scan time budget solving equation 5.17, potentially benefits from predicting multiple scans ahead, to improve its performance in the figure on the left in Figure 6.22.

  The formulation of a non-myopic cost function also introduces a trade-off between making an object presence decision at the current or future scans. This trade-off can be made by introducing a cost of making no decision in the current scan. [9]

- Considering the probability of object birth and death and the cost coefficients for a missed detection and false alarm as functions of time. In real scenarios, such parameters are rarely constant. Time-dependent parameters allow for more realistic application scenarios. For example, within a security surveillance application, the probability of object birth and object death is potentially different at night compared to daytime.
- Include the possibility of moving objects to allow for more realistic scenarios, as radars are often operated in highly dynamic environments. When moving objects are included, it is recommended to re-evaluate the assumption of a maximum of one object per range cell.

Bibliography

[1] Y. Li, W. Moran, S. Sira, A. Papandreou-Suppappola, and D. Morrell, "Adaptive waveform design in rapidly-varying radar scenes," 03 2009, pp. 263 – 267.

[2] J. Williams, "Search theory approaches to radar resource allocation," 06 2008.

[3] P. Boström-Rost, D. Axehill, and G. Hendeby, "Sensor management for search and track using the poisson multi-bernoulli mixture filter," *IEEE Transactions on Aerospace and Electronic Systems*, vol. 57, no. 5, pp. 2771–2783, 2021.

[4] G. E. Collins, M. M. Meloon, K. J. Sullivan, and J. Chinn, "An entropy-based approach to wide area surveillance," in *Signal Processing, Sensor Fusion, and Target Recognition XV*, I. Kadar, Ed., vol. 6235, International Society for Optics and Photonics. SPIE, 2006, p. 623509. [Online]. Available: https://doi.org/10.1117/12.663997

[5] F. Hoffmann and A. Charlish, "A resource allocation model for the radar search function," in *2014 International Radar Conference*, 2014, pp. 1–6.

[6] K. White, J. Williams, and P. Hoffensetz, "Radar sensor management for detection and tracking," in *2008 11th International Conference on Information Fusion*, 2008, pp. 1–8.

[7] D. J. Matthiesen, "Efficient beam scanning, energy allocation, and time allocation for search and detection," in *2010 IEEE International Symposium on Phased Array Systems and Technology*, 2010, pp. 361–368.

[8] M. Flint, E. Fernandez-Gaucherand, and M. Polycarpou, "Cooperative control for uav's searching risky environments for targets," in *42nd IEEE International Conference on Decision and Control (IEEE Cat. No.03CH37475)*, vol. 4, 2003, pp. 3567–3572 vol.4.

[9] Y. Wang, I. I. Hussein, and R. S. Erwin, "Risk-based sensor management for integrated detection and estimation," in *Proceedings of the 2011 American Control Conference*, 2011, pp. 3633–3638.

[10] M. Richards, J. Scheer, and W. Holm, *Principles of modern radar: Basic principles*, 01 2010.

[11] S. M. Kay, *Fundamentals of statistical signal processing: Detection theory*. Noida, India.: Dorling Kindersley (India), 2010.

[12] M. A. Richards, *Fundamentals of Radar Signal Processing*, 2nd ed. US: McGraw-Hill Professional, 2005. [Online]. Available: https://mhebooklibrary.com/doi/book/10.1036/0071444742

[13] H. V. Poor, *An Introduction to Signal Detection and Estimation (2nd Ed.)*. Berlin, Heidelberg: Springer-Verlag, 1994.

[14] T. de Groot, O. Krasnov, and A. Yarovoy, "Generic utility definition for mission-driven resource allocation," in *IET International Conference on Radar Systems (Radar 2012)*, 2012, pp. 1–5.

[15] B. Lambert, *A Student's Guide to Bayesian Statistics*. SAGE Publications, 2018. [Online]. Available: https://books.google.nl/books?id=di9wswEACAAJ

[16] R. Yates, *Probability and Stochastic Processes: A Friendly Introduction for Electrical and Computer Engineers, 3rd Edition: Third Edition*, ser. Probability and Stochastic Processes: A Friendly Introduction for Electrical and Computer Engineers. John Wiley & Sons, 2014. [Online]. Available: https://books.google.nl/books?id=zn5bAgAAQBAJ